




Please cite the Published Version

Lea-Carnall, Caroline A , El-Deredy, Wael , Stagg, Charlotte J, Williams, Stephen R and Trujillo-Barreto, Nelson J  (2023) A mean-field model of glutamate and GABA synaptic dynamics for functional MRS. *NeuroImage*, 266. 119813 ISSN 1053-8119

DOI: <https://doi.org/10.1016/j.neuroimage.2022.119813>

Publisher: Elsevier BV

Version: Published Version

Downloaded from: <https://e-space.mmu.ac.uk/634723/>

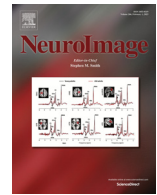
Usage rights:  [Creative Commons: Attribution-Noncommercial-No Derivative Works 4.0](https://creativecommons.org/licenses/by-nc-nd/4.0/)

Additional Information: This is an open access article which first appeared in *NeuroImage*, published by Elsevier

Data Access Statement: Data will be made available on request.

Enquiries:

If you have questions about this document, contact openresearch@mmu.ac.uk. Please include the URL of the record in e-space. If you believe that your, or a third party's rights have been compromised through this document please see our Take Down policy (available from <https://www.mmu.ac.uk/library/using-the-library/policies-and-guidelines>)



A mean-field model of glutamate and GABA synaptic dynamics for functional MRS

Caroline A. Lea-Carnall^{a,*}, Wael El-Deredy^{b,c,d}, Charlotte J. Staggs^{e,f}, Stephen R. Williams^{g,1}, Nelson J. Trujillo-Barreto^{a,1}

^a School of Health Sciences, Faculty of Biology, Medicine and Health, The University of Manchester, Manchester Academic Health Science Centre, UK

^b Centro de Investigación y Desarrollo en Ingeniería en Salud, Universidad de Valparaíso, Chile

^c Valencian Graduate School and Research Network of Artificial Intelligence.

^d Department of Electronic Engineering, School of Engineering, Universitat de València, Spain.

^e Wellcome Centre for Integrative Neuroimaging, FMRIB, Nuffield Department of Clinical Neurosciences, University of Oxford, Oxford, UK

^f MRC Brain Network Dynamics Unit, Nuffield Department of Clinical Neurosciences, University of Oxford, Oxford, UK

^g Division of Informatics, Imaging and Data Science, University of Manchester, Manchester, UK

ARTICLE INFO

Keywords:

Magnetic resonance spectroscopy
fMRS
Glutamate
GABA
Mathematical modelling
Mean field model

ABSTRACT

Advances in functional magnetic resonance spectroscopy (fMRS) have enabled the quantification of activity-dependent changes in neurotransmitter concentrations in vivo. However, the physiological basis of the large changes in GABA and glutamate observed by fMRS (>10%) over short time scales of less than a minute remain unclear as such changes cannot be accounted for by known synthesis or degradation metabolic pathways. Instead, it has been hypothesized that fMRS detects shifts in neurotransmitter concentrations as they cycle from presynaptic vesicles, where they are largely invisible, to extracellular and cytosolic pools, where they are detectable. The present paper uses a computational modelling approach to demonstrate the viability of this hypothesis. A new mean-field model of the neural mechanisms generating the fMRS signal in a cortical voxel is derived. The proposed macroscopic mean-field model is based on a microscopic description of the neurotransmitter dynamics at the level of the synapse. Specifically, GABA and glutamate are assumed to cycle between three metabolic pools: packaged in the vesicles; active in the synaptic cleft; and undergoing recycling and repackaging in the astrocytic or neuronal cytosol. Computational simulations from the model are used to generate predicted changes in GABA and glutamate concentrations in response to different types of stimuli including pain, vision, and electric current stimulation. The predicted changes in the extracellular and cytosolic pools corresponded to those reported in empirical fMRS data. Furthermore, the model predicts a selective control mechanism of the GABA/glutamate relationship, whereby inhibitory stimulation reduces both neurotransmitters, whereas excitatory stimulation increases glutamate and decreases GABA. The proposed model bridges between neural dynamics and fMRS and provides a mechanistic account for the activity-dependent changes in the glutamate and GABA fMRS signals. Lastly, these results indicate that echo-time may be an important timing parameter that can be leveraged to maximise fMRS experimental outcomes.

1. Introduction

Understanding how neurochemistry affects human physiology in health and disease is of central importance to clinical and neuroscientific

fields. However, the need for non-invasive methods to quantify neurotransmitter activity in humans makes this question inherently challenging. Magnetic resonance spectroscopy (MRS) allows quantification of brain metabolites non-invasively, providing a method to directly mea-

Abbreviations: AMPA, α -amino-3-hydroxy-5-methyl-4-isoxazolepropionic acid; ECS, extracellular space; E, excitatory; fMRS, functional magnetic resonance spectroscopy; GABA, γ -aminobutyric acid; GAD, glutamic acid decarboxylase; Gln, glutamine; Glu, glutamate; Glx, the sum of glutamine plus glutamate; HH, Hodgkin-Huxley; I, inhibitory; MFM, mean-field model; mM, millimolar; MRI, magnetic resonance imaging; MRS, magnetic resonance spectroscopy; NAA, N-acetylaspartate; NMDA, N-methyl-D-aspartate; NT, neurotransmitters; PAG, phosphate activated glutaminase; SD, standard deviation; SE, standard error; SNR, signal-to-noise ratio; TCA, tricarboxylic acid cycle; tCr, total creatine, the sum of creatine plus phosphocreatine; tDCS, transcranial direct current stimulation.

* Corresponding author.

E-mail addresses: caroline.lea-carnall@manchester.ac.uk (C.A. Lea-Carnall), wael.el-deredy@uv.cl (W. El-Deredy).

¹ Joint senior authors

<https://doi.org/10.1016/j.neuroimage.2022.119813>.

Received 9 August 2022; Received in revised form 31 October 2022; Accepted 13 December 2022

Available online 14 December 2022.

1053-8119/© 2022 Published by Elsevier Inc. This is an open access article under the CC BY-NC-ND license (<http://creativecommons.org/licenses/by-nc-nd/4.0/>)

sure the concentrations of the brain's major neurotransmitters (NT), glutamate (Glu), and γ -aminobutyric acid (GABA) in vivo (Rae, 2014). However, it is not clear how to interpret the resulting signals in terms of the underlying cellular mechanisms. Here, we use mean-field theory to provide a macroscopic level account of the basis of Glu and GABA functional MRS (fMRS) signal changes in response to stimulation. We then use the model to predict the precise metabolic pools that give rise to activity-dependent changes in the fMRS signal.

Traditionally, MRS has been used to provide a static snapshot of neurotransmitter levels in the brain, predominantly used to allow comparison between healthy and diseased states. However, there is increasing use of MRS to quantify time-resolved metabolic responses to stimuli on much shorter timescales of seconds to minutes, so-called *functional* MRS (see (Jelen et al., 2018; Mullins, 2018) for reviews). Following earlier work in the visual system, fMRS applications have now been expanded to a range of other paradigms including motor, cognitive, and pain stimuli (as reviewed by Jelen et al., 2018; Mullins, 2018). In many of these studies, the authors report changes in neurochemical concentration of 10–14% in response to short bouts of stimulation. In addition to studies focussed on healthy volunteers, the utility of fMRS techniques in clinical populations is also increasingly being explored. For example, a recent fMRS study in the anterior cingulate cortex showed that the expected increase in Glu in response to a Stroop task was significantly reduced in people with schizophrenia and major depressive disorder (Taylor et al., 2015). Given that this region has been substantially implicated in schizophrenia, with increased Glu and glutamine (Gln) levels observed commonly, fMRS is therefore able to significantly aid our understanding of the pathophysiological processes of these complex diseases (Bustillo et al., 2010; Théberge et al., 2002). Therefore, understanding the physiological basis for differences in the neurochemical response between healthy and diseased states is crucial to optimize clinical treatments.

MRS uses technology similar to magnetic resonance imaging (MRI), but the MRS signal is directly proportional to the concentration of metabolites within the specified region of interest (voxel). Nonetheless, the physiological basis of activity-dependent changes in the fMRS neurotransmitter signal remains unclear (Jelen et al., 2018; Mullins, 2018). Focusing on Glu initially, the most widely-accepted explanation is that an increased MRS-Glu signal reflects increased metabolic turnover (for example, via the anaplerotic pathway) (Rothman et al., 2003). However, it remains controversial as to whether these processes are able to account for the large changes observed in the MRS signal (>5%) over short time scales of seconds to minutes (Jelen et al., 2018; Mullins, 2018). For example, (Jelen et al., 2018) argue that changes in Glu of 6% or more in a minute cannot be explained by synthesis/degradation, since calculations based on the cerebral metabolic rate of glucose utilisation 0.26 mM min^{-1} (Hyder et al., 2016) could not produce the same magnitude of change in such a short time (even under the unrealistic assumption that all glucose is metabolized to glutamate). For reference, we note that if functional changes in Glu represent newly synthesized glutamate, which removes carbon from the cycle, it must be replaced by anaplerosis. Using known rates of glutamate synthesis from (Shen et al., 1999), an acquisition duration of 5 mins would yield synthesis of Glu via the anaplerotic pathway to account for an increase of 0.2 mM. These relate to an increase of 2% assuming an average concentration of 10 mM in the human brain, less if degradation was also taken into account.

A major source of neuronal Glu is via flux through the Glu-Gln cycle, which has been shown in animals to exhibit rate increases in response to neural stimulation and thus can reasonably be expected to do the same in humans (Sibson et al., 1998). Upon exocytosis into the cleft, Glu is quickly taken up by nearby astrocytes and converted to Gln (a non-neuroactive species), Gln is then returned to the neuron where it is converted back to Glu and packaged into vesicles (Mangia et al., 2012). Supported by observations of varying Glu-MRS visibility in different compartments (Kauppinen et al., 1994; Kauppinen and Williams, 1991; Pirttilä et al., 1993) and on the echo-time dependence of fMRS signal

changes, Jelen et al. proposed that fMRS detects compartmental shifts (in Glu) due to neural activation, as it moves from pre-synaptic vesicles to more visible synaptic, extracellular and astrocytic pools (Jelen et al., 2018). Glu will naturally cycle through these compartments as it passes through the stages of release, reuptake and vesicular repackaging in response to neural firing. It has been estimated that up to 30% of Glu is invisible to MRS at any one time (Kauppinen et al., 1994; Kauppinen and Williams, 1991; Pirttilä et al., 1993) due to it being tightly bound to macromolecular structures in the vesicles, including monotypic, polytypic, and associated membrane proteins (Südhof, 1999), causing faster T2 relaxation (Kauppinen et al., 1994; Kauppinen and Williams, 1991). In the case of the inhibitory transmitter GABA, the process is less complex in that released GABA is returned to the presynaptic cell largely via reuptake mechanisms where it is repackaged into vesicles (Olsen and DeLorey, 1999). Vesicle refilling has been shown to occur in an activity-dependent manner (Li et al., 2020). Importantly, maximal rates of release and refilling are not equivalent; for example in a hippocampal slice experiment, it was estimated that quanta are released from occupied sites at a rate of 0.72 s^{-1} , whereas the rate of refilling an empty site occurs at the rate 0.11 s^{-1} . Therefore, it could be that neural activation drives a shift of Glu (or GABA) between states that are more or less visible to MRS via the recycling processes described above and that this shift between states contributes to the change in fMRS signal at short time scales. Here, we develop a neural mass model with compartmental NT dynamics to investigate how changes in neural activity might affect the fMRS signal under the hypothesis that vesicular NT contributes minimally to the MRS signal at standard echo times used empirically. Specifically, we wish to test how much of the fMRS signal change can be explained by shifting of NT between compartments over short timescales of less than 1 min. We interrogate the model with a range of stimulation types intended to mimic visual, pain, and transcranial direct current stimulation (tDCS) and test the model predictions against empirical data found in the literature. The model allows us to link cellular level mechanisms of neural activity and NT dynamics with their systems-level observations via the MRS signal.

To achieve this, we develop a model of interacting populations of excitatory (E) and inhibitory (I) neurons intended to represent a generic cortical MRS voxel. We start with a microscopic-level model of neural activity based on the well-established Hodgkin-Huxley formalism (Hodgkin and Huxley, 1952). We explicitly incorporate a multi-compartment description of the movement of neurotransmitters between pools based on work by Tsodyks and Markram (Tsodyks and Markram, 1997). This multi-compartment model of NT dynamics assumes a fixed absolute quantity of NT that cycles between three pools: effective, inactive or readily releasable in an activity-dependent manner. We interpret these pools to correspond to, respectively, NT found instantaneously in the cleft upon cell activation or in the extracellular space (ECS); NT undergoing recycling or other biological processes (cytosolic compartment); and NT packaged in vesicles ready for release. Essentially, the model accounts for the simplified dynamics of the release-reuptake-repackaging cycles described above. We obtain a macroscopic systems-level approximation of the neurotransmitter activity by deriving the mean-field reduction of the system dynamics under the Laplace approximation (Marreiros et al., 2008, 2009). This allows us to formulate a description of the average response of a population of neurons to stimulation and the associated population-level changes in NT concentrations where the population density assumes a Gaussian form. We do not account for absolute (total) changes in NT concentration due to metabolic flux over the short timescales under investigation here as it is our aim to understand how much of the change in MRS signal could theoretically be accounted for by considering only the movement of NT between compartments of differing MR-visibility.

We simulated three types of stimuli to apply to the model: acute pain, visual, and current stimulation to emulate the most common fMRS studies. We used the model output to make predictions about how the cells microscopic activity translates to changes in the fMRS measurement un-

der the assumption that the vesicular pool of NT exhibits very short T2 relaxation and therefore contributes minimally to the overall signal at standard echo times found in the literature. Finally, we compare our findings to empirical data. In doing so, we provide a mechanistic account for the change in observed NTs concentrations during cognitive fMRS studies.

2. Theory

We model a cortical region as a local network composed of two densely interconnected populations of spiking excitatory and inhibitory neurons. The neurons are coupled through excitatory α -amino-3-hydroxy-5-methyl-4-isoxazolepropionic acid (AMPA) and inhibitory (GABA) synapses. Glu acts on postsynaptic AMPA receptors to excite the cell and depolarise it, whereas GABA acts on GABA receptors to hyperpolarise and inhibit the cell. A key component of the spiking model is that we account for the dynamics of both GABA and Glu during synaptic transmission. This allows us to study how the dynamics of the NT themselves vary in response to stimulation and predict how the functional MRS signal in turn would be affected.

Our aim is to relate the NT activity in the model to MRS-derived measurements of GABA and Glu, which are acquired over large voxels in the brain containing billions of neurons. Using a network model comprised of individual cells, this would entail simulating considerable numbers of coupled nonlinear differential equations. Rather, we derive a mean-field reduction of the spiking network model. This reduction describes the evolution of the ensemble of neurons representing a local population, in terms of the dynamics of the average states of the ensemble. We follow Marreiros *et al.* to approximate the average ensemble behaviour under the Laplace approximation (Marreiros *et al.*, 2008, 2009), see Appendix for derivation.

2.1. Microscopic model dynamics

2.1.1. Extended Hodgkin-Huxley model

We begin by defining the equations governing the behaviour of the individual neurons that comprise the network. Experimentally, it has been found that neocortical pyramidal cells exhibit dense reciprocal connectivity within a local region as well as strong connections with pyramidal cells in different regions via AMPA and N-methyl-D-aspartate (NMDA) receptor-mediated transmission (Czeiger and White, 1993; Elhanany and White, 1990; Johnson and Burkhalter, 1996; Mountcastle 1997; Somogyi *et al.*, 1998; Szentágothai, 1983). Inhibitory cells receive excitatory input from pyramidal cells mainly via AMPA receptor-mediated transmission (Bartos *et al.*, 2007). Similarly, GABAergic synapses have been found to mediate inhibitory connections on to pyramidal cells and inhibitory basket cells (Freund and Katona, 2007; Molaee-Ardekani *et al.*, 2010). Therefore, we base the model structure on these principles and define 2 populations of cells; an excitatory population and an inhibitory population coupled via AMPA, and GABA-mediated connections. We note that the inclusion of NMDA receptors did not substantially alter the model behaviour and therefore were omitted. The E-population has N_E neurons, and the I-population has N_I neurons.

A single neuron is modelled using an extended form of the classical Hodgkin-Huxley (HH) neuronal model (Hodgkin and Huxley, 1952). This model was chosen so as to be able to tune the excitatory and inhibitory neurons with data acquired directly from the biology (using (Pospischil *et al.*, 2008)) in order to test the effect of stimulation on the biologically realistic networks. The HH model is a conductance model that describes the evolution of the membrane potential of a neuron as being the sum of currents which pass through the cell membrane. The standard HH model accounts for leak, sodium and potassium currents, and we have extended the model to include AMPA and GABA-receptor-mediated currents in addition to this. The standard equations describing the evolution of the membrane potential for a single HH neuron j are given by (adapted from (Pospischil *et al.*, 2008), see also (Destexhe,

1997; Kobayashi and Kitano, 2016)), where $\dot{x}(t)$ is the time derivative of x at time t :

$$C\dot{V}_j^\alpha(t) = I_{int,j}^\alpha(t) - I_{ext,j}^\alpha(t) - I_{A,j}^\alpha(t) - I_{G,j}^\alpha(t) - I_0^\alpha \quad (1)$$

where

$$I_{int,j}^\alpha(t) = -g_L(V_j^\alpha(t) - V_L^\alpha) - g_{Na}^\alpha m^{\alpha 3}(t)h^\alpha(t)(V_j^\alpha(t) - V_{Na}^\alpha) - g_K^\alpha n^{\alpha 4}(t)(V_j^\alpha(t) - V_K) \quad (2)$$

$$I_{A,j}^\alpha(t) = g_A(V_j^\alpha(t) - V_R^A) \sum_{k=1}^{N_E} w_{E\alpha} \gamma_{jk}^E p_k^A(t) \quad (3)$$

$$I_{G,j}^\alpha(t) = g_G(V_j^\alpha(t) - V_R^G) \sum_{k=1}^{N_I} w_{I\alpha} \gamma_{jk}^I p_k^G(t) \quad (4)$$

In Eqs. (1) to (4), V_j^α where $\alpha \in \{E, I\}$ denotes the membrane potential of an excitatory or inhibitory cell j respectively. Where α does not appear as a superscript for a variable, this implies that the parameter is the same regardless of the cell type. All parameter values are listed in Table 1. Changes in the membrane potential are driven by incoming signals from connected excitatory and inhibitory neurons k in the form of GABA and Glu concentrations in the cleft, as well as external current-based inputs. C is the specific capacitance of the membrane; $I_{ext,j}$ is the external input current; $I_{int,j}$ encompasses the voltage-dependent leak, sodium and potassium currents, respectively, which are responsible for the action potential generation; $g_L, g_{Na}^\alpha, g_K^\alpha$ are the mean leak, sodium and potassium conductances; $V_L^\alpha, V_{Na}^\alpha, V_K$ are the associated reversal potentials. The voltage-mediated gating variables $m, n,$ and h represent the fraction of open channels of each current type and are represented by standard exponential functions detailed in the Appendix. In order for the model to generate activity we added an extra input term I_0^E to the excitatory population only for all simulations as without this input the model does not generate spontaneous activity, similar to (Kobayashi and Kitano, 2016; Pospischil *et al.*, 2008). The synaptic input currents are given by the AMPA (I_A), and GABA (I_G) receptor mediated synaptic input currents which will have either an excitatory or inhibitory effect on the cell. Following (Zou and Destexhe, 2007), we consider GABA_A receptors only as the majority of inhibitory postsynaptic potentials are mediated by GABA_A receptors (Destexhe, 1997). They are highly sensitive to GABA and can be fully saturated by GABA released from a single vesicle; whereas GABA_B require stronger stimuli to respond (Destexhe, 1997 *et al.*, 1994; Thompson, 1994). The respective mean synaptic conductances are $g_A,$ and g_G ; with V_R^A, V_R^G representing the AMPA and GABA receptor reversal potentials. The binary connectivity matrices γ^E and γ^I represent maps of excitatory or inhibitory connections between neurons, so $\gamma_{j,k}^\alpha$ is the (j, k) element of the matrix which is equal to 1 if neuron j is connected to k , and 0 otherwise. $w_{E\alpha}, w_{I\alpha}$ are the dimensionless parameters that represent the synaptic weights between the cell types, as in (Deco *et al.*, 2014). p_k^A and p_k^G are the synaptic gating variables for each connected synapse k and depend on the population type (excitatory and inhibitory, respectively).

The synaptic gating variables p for AMPA and GABA mediated channels are given by the following kinetic differential equation (Destexhe, 1997):

$$\dot{p}_k^\beta(t) = a^\beta b_k^\alpha(t)(1 - p_k^\beta(t)) - c^\beta p_k^\beta(t) \quad (5)$$

Where $\beta \in \{A, G\}$ denotes the type of synaptic receptor (AMPA or GABA), b_k^α represents the concentration of active NT acting instantaneously on receptor type β in the synaptic cleft of an afferent connection from a neuron k of population α where $\alpha \in \{E, I\}$ and relates to Glu or GABA respectively. Finally, a^β and c^β are rate constants specified in Table 1.

In standard conductance-based models, the synaptic currents are a function of the firing of presynaptic neurons, which are in turn functions of the membrane potentials. Closing this loop allows for the membrane

potential to be determined self-consistently. However, this type of modelling sidesteps the explicit modelling of neurotransmitter dynamics. In our case, for the membrane potential to be computed self-consistently, the dynamics of the neurotransmitters need to be expressed as a function of the pre-synaptic firing. In the next section, we describe the equations governing neurotransmitter cycling activity.

2.1.2. Neurotransmitter cycling

Upon activation, excitatory neurons release Glu into the postsynaptic cleft which rapidly binds to postsynaptic receptor sites and then is very quickly taken up by surrounding astrocytes. Within astrocytes Glu is amidated to Gln by glutamine synthetase and released into the extracellular space. Gln, a non-neuroactive species, is then taken up by the presynaptic neuron where it is converted back into Glu via phosphate-activated glutaminase (PAG) and repackaged into vesicles. In addition to this, cytosolic Glu concentrations are also synthesised by the anaplerotic pathway via the tricarboxylic acid cycle (TCA) cycle.

In the case of inhibitory cells, released GABA is primarily taken up at the presynaptic terminal ready to be repackaged into vesicles. Synaptic GABA is also taken up into astrocytes where it is metabolised via the TCA cycle to succinate and then to Glu and finally Gln. In a similar way to the glutamatergic synapse, Gln is then released into the extracellular space and transported back to the presynaptic cell where it is converted back to Glu via PAG and finally to GABA via glutamic acid decarboxylase (GAD) after which it is packaged into vesicles ready for re-release. In addition to these two processes, cytosolic GABA is also synthesised by the anaplerotic pathway via TCA cycle as in the glutamatergic cell.

In this paper, we do not account for absolute changes in NT concentration due to metabolic flux in response to stimulation. Instead, we focus on movement of NT between cellular environments that are more or less visible to MRS to ascertain whether this shift in concentration is enough to explain the magnitude of change that we observe in the MRS signal over short timescales.

To account for the above mechanisms surrounding neurotransmitter recycling in the model, we make the following assumptions:

1. Neurotransmitter is released into the cleft in an activity-dependent manner and is rapidly removed so that it can no longer act on the postsynaptic cell.
2. Once removed from the cleft, neurotransmitter is assimilated into the cytosolic neurotransmitter concentration.
3. Cytosolic neurotransmitter is then repackaged into the vesicles; the temporal evolution of this process depends on both the level of cytosolic transmitter and neural activity (Li et al., 2020).

We note here that for Glu, the situation is more complex as it is recycled via astrocytic conversion to Gln. Accounting for this extra step is an area for further work but we note here that in many MRS studies the combined measure Glx (which includes the Glu and Gln peaks) is used to approximate the Glu concentration and in these cases the model predictions are particularly relevant. Additionally, we note that Glu is present in approximately 4 times the concentration of Gln in the brain (see Ramadan et al., 2013).

We employ the kinetic model of Tsodyks and Markram (Tsodyks and Markram, 1997) which characterises the transition of NT between the 3 states: R (the fraction of releasable transmitter in the bouton - the vesicular pool), X (the fraction of effective transmitter in the cleft) and N (the remaining proportion of "inactive" transmitter which for our purposes we assume to be cytosolic neurotransmitter awaiting repackaging into vesicles), see Fig. 1. For each spike, a proportion of NT is released from the vesicles into the cleft after which it is cleared, returned to the cytosol and repackaged into the vesicles. The equations describing the temporal evolution of NT in each compartment (for an excitatory cell the equations describe Glu cycling, and for inhibitory cells GABA cycling) for cell k are given by:

$$\dot{R}_k^\alpha(t) = \frac{f(N_k^\alpha(t) - N_0)}{\tau_r} - UR_k^\alpha(t) \sum_q \delta(t - t_q^k) \quad (6)$$

$$\dot{X}_k^\alpha(t) = -\frac{X_k^\alpha(t)}{\tau_x} + UR_k^\alpha(t) \sum_q \delta(t - t_q^k) \quad (7)$$

$$N_k^\alpha(t) = 1 - R_k^\alpha(t) - X_k^\alpha(t) \quad (8)$$

$$b_k^\alpha(t) = BX_k^\alpha(t) \quad (9)$$

where

$$f(x) = xH(x) \quad (10)$$

Where Eq. (8) is a conservation rule ensuring that the total amount of NT at any point in time is constant, and $\sum_q \delta(t - t_q^k)$ denotes the spike train of presynaptic neuron k firing action potentials at times q . With each presynaptic spike, a fraction U of the total available neurotransmitter stored in the vesicles (R) is released into the cleft/ECS (X). NT is cleared from the cleft with time constant τ_x and is assimilated in the cytosol (N) via Eq. (8). The transmitter in the cytosol (N) undergoes recycling and repackaging into the vesicles at a rate τ_r . H in Eq. (10) is the Heaviside function and determines when the cytosolic compartment has reduced to 70% under which no further repackaging can occur. Eqs. (6) to (8) describe the proportion of the total NT in each of the pools which are multiplied by an absolute concentration, B , to convert the proportion of NT to a concentration in the cleft into a concentration in mM, denoted b_k^α (Eq. (9)). Therefore, the concentration of neurotransmitter acting on the postsynaptic cell j (via Eq. (5)) from presynaptic cell k is given by $BX_k^\alpha(t)$. As before, $\alpha \in \{E, I\}$ determines whether NT is Glu or GABA. We adapt the model by including a lower bound N_0 set to 70% (Eq. (6)) which defines a lower bound to the fraction of cytosolic NT below which no further vesicular packaging occurs (and can practically be thought of as ensuring that no more than 30% of the total NT is packaged in the vesicles, based on (Kauppinen et al., 1994; Kauppinen and Williams, 1991; Pirttilä et al., 1993).

As there is a considerable mismatch between the rate of exocytosis and the rate of recycling into the vesicles ready for release, a natural consequence of these equations is that during increased stimulation there is a shift of transmitters from a relatively MR-invisible compartment (vesicles) to a detectable compartment in the cytosol of astrocytes and neurons resulting in an increased MRS signal for that metabolite (see Fig. 1). The opposite effect occurs when firing is reduced.

2.2. Macroscopic model dynamics

2.2.1. Mean-Field model

A typical MRS signal is acquired from a large voxel of brain tissue (in the region of cm^3) making it a macroscopic measure of activity. The goal of this paper is to describe the evolution of NT dynamics in terms of what is measured using MRS and therefore the model must also account for activity at this spatial scale. So far, the model equations account for the activity of a neuron. To model the behaviour of a network of billions of connected neurons using these equations would be computationally prohibitive. Rather, we derive a mean-field reduction of these large-scale neuronal network under the Laplace approximation following (Marreiros et al., 2008, 2009), please see Appendix for details. This method allows us to look at the average activity over a large population of cells rather than modelling each cell individually and is a method borrowed from statistical physics commonly used to simplify neural network computation meaning that we can make meaningful comparisons between the model output and the MRS signal obtained from a neural network contained within typical voxel.

The Laplace approximation allows us to summarise the density dynamics of an ensemble of neurons using the method of moments (Rodriguez and Tuckwell, 1996, 1998) where the population density assumes a fixed Gaussian form. The mean-field model (MFM) expresses the time evolution of the mean activity of each population of neurons

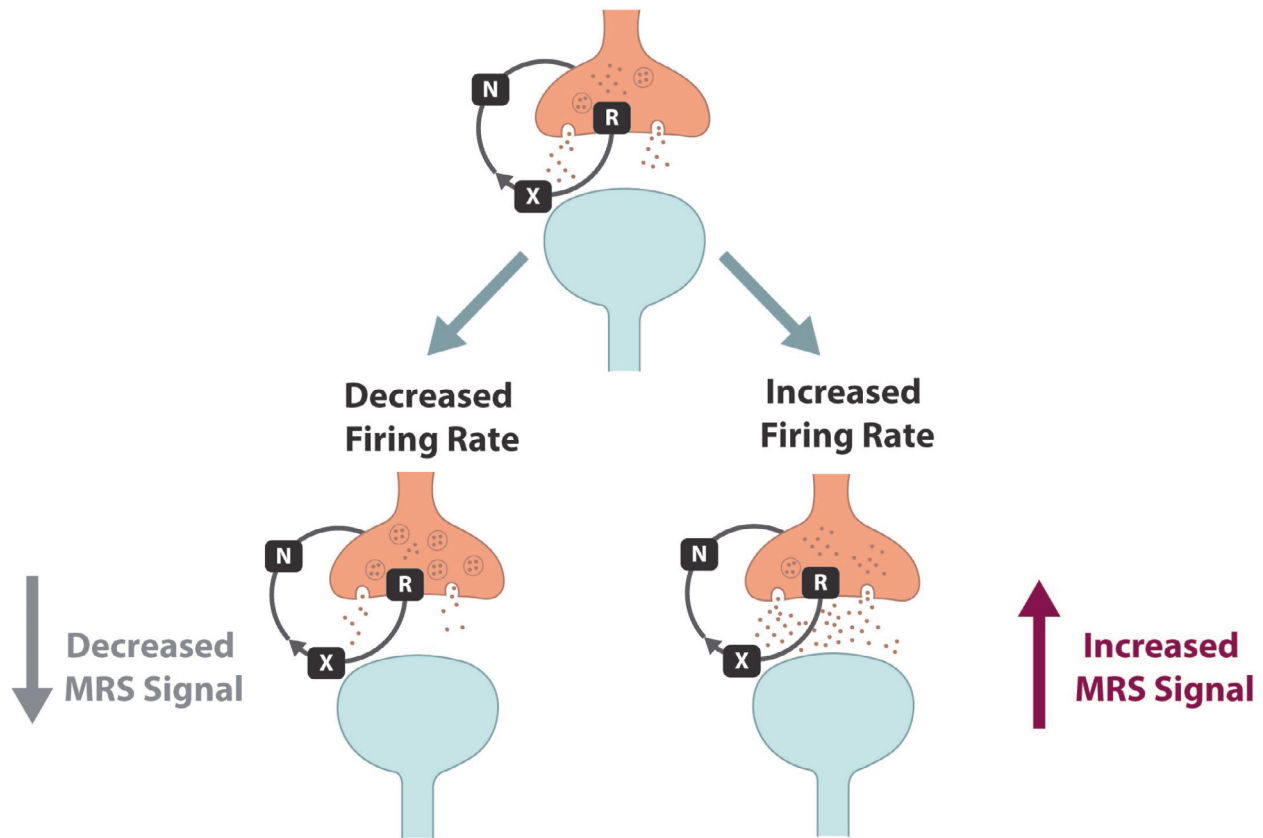


Fig. 1. Neurotransmitter cycling Schematic diagram of generalised NT cycling process as per the kinetic model of Tsodyks and Markram (Tsodyks and Markram, 1997). The presynaptic cell is shown in pink and the postsynaptic in blue. Steady state (top): the presynaptic cell fires an action potential releasing NT (GABA or Glu) into the cleft. NT is characterised as belonging to one of three states: NT in the vesicular pool (R), where the NT is packaged in the vesicles ready to be released into the cleft upon activation; NT in the extracellular space (X), where it has been released into the cleft and is acting at receptor sites on the postsynaptic cell; and NT in the cytosolic pool (N), is awaiting repackaging into the vesicles. Decreased firing (left): if the firing rate is reduced, the NT will start to accumulate in the vesicles due to the mismatch between the rate of exocytosis and the rate of repackaging into the vesicles. A shift of NT from the cytosol to the vesicles will result in a decreased MRS signal as we assume the vesicular compartment is largely invisible to MRS. Increased firing (right): if the firing rate increases, then NT from the vesicles will be used more quickly. Upon exocytosis it will transfer rapidly from the cleft to the cytosol and start to accumulate there. A shift of NT from the vesicles to the ECS and the cytosol will result in an increased MRS signal under the current hypothesis.

(excitatory and inhibitory) within the local spiking network described previously by averaging over the activity of all cells within each population. This is achieved by expressing the state variables by their mean values and replacing the sum over spikes found in (Eqs. (6) to (7)) with an averaged value (firing rate) calculated using a sigmoidal input-output function (Abbott and Chance, 1995). The key point to note is that under the mean field assumption, the states of all neurons in a population are affected by the averaged state of all neurons in a connected population. It is not possible for a single neuron in a population to directly affect another individual neuron in the same or another population. In the MFM, we consider only the first statistical moment of the distribution, the mean, while discounting higher order moments thus equating the system to a neural mass model (Marreiros et al., 2009). The model architecture, intended to account for a generic cortical voxel, comprises an excitatory and an inhibitory population of cells, these are both self- and inter-connected, see Fig. 2. Both populations are capable of receiving excitatory (AMPA receptor-mediated) and inhibitory (GABA receptor-mediated) inputs.

Under the mean-field assumption and Laplace approximation, the equations have a similar structure and parameter interpretation as in the single-neuron model, but with state variables replaced with their population averages and the input train of spikes replaced by a sigmoidal activation function. The equations of motion for the means of the state variables for each population $\alpha \in \{E, I\}$ are given below where μ_x de-

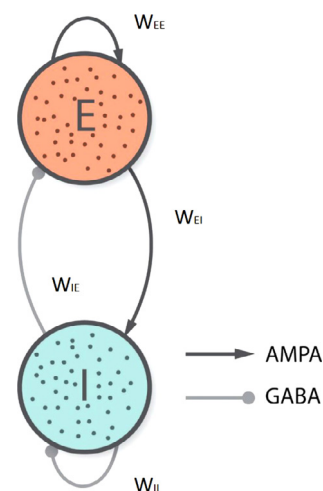


Fig. 2. Schematic of the mean-field model The MFM is intended to approximately represent a generic cortical MRS voxel. It consists of an excitatory (E) and inhibitory (I) population representing the averaged activity of billions of cells. These are both self and inter-connected via the weights $w_{EE}, w_{II}, w_{EI}, w_{IE}$. All connection strengths are fixed. Inhibitory connections are mediated via GABA receptors and excitatory connections via AMPA receptors.

defines the mean-field quantity for variable x :

$$C\dot{\mu}_V^\alpha(t) = I_{int}^\alpha(t) - I_{ext}^\alpha(t) - w_{E\alpha}I_A^\alpha(t) - w_{I\alpha}I_G^\alpha(t) - I_0^\alpha \quad (11)$$

$$I_{int}^\alpha(t) = -g_L(\mu_V^\alpha(t) - V_L^\alpha) - g_{Na}^\alpha\mu_m^{\alpha 3}(t)\mu_h^\alpha(t)(\mu_V^\alpha(t) - V_{Na}) - g_K^\alpha\mu_n^{\alpha 4}(t)(\mu_V^\alpha(t) - V_K) \quad (12)$$

$$I_A^\alpha(t) = g_A(\mu_V^\alpha(t) - V_R^A)\mu_p^A(t) \quad (13)$$

$$I_G^\alpha(t) = g_G(\mu_V^\alpha(t) - V_R^G)\mu_p^G(t) \quad (14)$$

$$\dot{\mu}_p^\beta(t) = a^\beta b^\alpha(t)(1 - \mu_p^\beta(t)) - c^\beta \mu_p^\beta(t) \quad (15)$$

$$\dot{\mu}_R^\alpha(t) = \frac{f(\mu_N^\alpha(t) - N_0)}{\tau_r} - U\mu_R^\alpha(t)S(\mu_V^\alpha(t), \sigma_V) \quad (16)$$

$$\dot{\mu}_X^\alpha(t) = -\frac{\mu_X^\alpha(t)}{\tau_x} + U\mu_R^\alpha(t)S(\mu_V^\alpha(t), \sigma_V) \quad (17)$$

$$S(\mu_V^\alpha, \sigma_V) = \frac{V_{max}}{1 + \exp((V_{tr} - \mu_V^\alpha(t))/\sigma_V)} \quad (18)$$

Variables x are as defined previously with μ_x representing their mean-field quantity with $\alpha \in \{E, I\}$ and $\beta \in \{A, G\}$ where E and I refer to the excitatory and inhibitory populations and A and G to AMPA and GABA receptor types. For example, $\mu_V^\alpha(t)$ defines the mean membrane potential for population α at time t . I_{int} refers to the voltage-mediated currents, I_{ext} , I_0 determine the external input currents, and I_A , I_G refer to the AMPA and GABA-receptor mediated currents. C is the mean membrane capacitance, the mean conductances g_L , g_{Na}^α , g_K^α , g_A , g_G and reversal potentials V_L^α , V_{Na} , V_K , V_R^A , V_R^G for the leak, Na, K, AMPA and GABA currents are as previously defined. Likewise, μ_m^α , μ_h^α , μ_n^α , μ_p^A , μ_p^G define the mean synaptic gating variables for each conductances (standard equations representing the initial three are detailed in the [Appendix](#)). μ_X^α , μ_R^α , μ_N^α define the mean proportion of NT in each of the compartments X , R , N for each population. NT is cleared from the cleft with time constant τ_x , and undergoes repackaging into the vesicles at a rate τ_r . Here the weights $w_{E/I}$ denote the coupling strength between the populations. The values for w and I_0 were chosen to obtain spontaneous activity for each population, as in ([Deco et al., 2014](#)).

S is a sigmoidal function which transforms the mean membrane potential of all cells within a population to an averaged firing rate. Essentially, it represents the cumulative distribution of the membrane's depolarisation (or its deviation from resting levels) under Gaussian assumptions with mean μ_V^α and variance σ_V . V_{max} relates to the maximal firing rate of the presynaptic cells which is normalised to 1 as in ([Wilson and Cowan, 1972, 1973](#)), for example, and can be thought of as converting the mean membrane potential to a fractional (percentage) firing rate. V_{tr} is a voltage threshold that defines the point at which the function is half-activated, while σ_V determines the steepness of the curve. We also note that in the present study, all connections are assumed to be instantaneous and therefore conduction delays between distant cortical areas are neglected. The full system of equations can be found in the [Appendix](#) and parameter values in [Table 1](#).

3. Methods and materials

3.1. Input types

Understanding how stimulation interacts with ongoing brain dynamics is important to optimise therapeutic and rehabilitation strategies ([Malerba et al., 2017](#)). In order to generate model predictions for a range of experimental scenarios, we modelled three different stimulus input

types. These were: tDCS, as it allows the inclusion of negative/inhibitory inputs; visual stimulation, as this is one of the most common stimulus types used in fMRS studies; and pain, as painful stimuli have been shown to elicit the largest changes in Glu and GABA in fMRS studies ([Mullins, 2018](#)). The major distinction between the input types is which cell population is targeted by the stimulation. Beyond that, we note that current stimulation is not thought to induce cell firing, so must be less than 5 mA as that is the minimum input required to cause excitatory cell firing in the model. Therefore, we consider sensory stimulation to occur for stimulus intensities greater than 5 mA in the current model.

3.1.1. Electrical stimulation (tDCS)

To model the effects of tDCS, we applied the stimulus to both the excitatory and inhibitory populations following ([Molae-Ardekani et al., 2021](#)) who recently showed that extending a tDCS-style input to inhibitory interneurons as well as excitatory pyramidal cells allowed them to simulate evoked potentials that were much closer to physiological data. Here we used $I_{ext}^I = 0.5I_{ext}^E$ as in ([Bonaiuto and Bestmann, 2015; Molae-Ardekani et al., 2021](#)). We note that the effects of electrical stimulation depend on a number of factors such as current field and cell orientation ([Berzhanskaya et al., 2013; Rahman et al., 2015; Tranchina and Nicholson, 1986](#)), and acknowledge that this is an area for future work.

3.1.2. Visual stimulation

To model vision, we applied the input only to the excitatory population, as in ([Wilson, 2003](#)), formally $I_{ext}^I = 0$. We account for the temporal properties of visual stimuli and allow the stimulus to flicker at 2 Hz.

3.1.3. Pain

To model acute pain, we applied a depolarising stimulus equally to both the excitatory and inhibitory populations of the model following ([Song et al., 2021](#)), formally $I_{ext}^I = I_{ext}^E$. We do not account for the temporal properties of the stimulus as these are beyond the scope of this paper.

3.2. Observation model

In this paper, we focus on 1H-MRS which is commonly used to analyse the chemical composition of tissue in vivo with the resulting signal reported as an average over the tissue volume and in time. The mean-field model presented here determines the distribution of NT in each of the 3 compartments at any point in time. The predicted MRS signal for each metabolite then is the time average (over the recording period) of the sum of the signal of the 3 compartments. The predicted signal $S_c^\alpha(t)$ at time t for compartment $c \in \{X, R, N\}$ and each metabolite $\alpha \in \{\text{Glu}, \text{GABA}\}$ is calculated using the Bloch Equation ([Bloch, 1946](#)):

$$S_c^\alpha(t) = \Phi_c^\alpha(t)(1 - e^{-TR/T1})e^{-TE/T2_c^\alpha} \quad (19)$$

Where TR is the scan repetition time, $T1$ is the longitudinal relaxation rate, TE is the echo time, and $T2_c^\alpha$ is the compartment-specific transverse relaxation rate for each metabolite (see [Table 1](#) for values reported at 3 Tesla). Φ_c^α is the effective spin density for each compartment which is modelled as the corresponding compartmental fraction of the total spin density for the voxel Φ_0^α , so that $\Phi_c^\alpha(t) = \mu_c^\alpha(t)\Phi_0^\alpha$. $\Phi_0^\alpha(t)$ can be thought of as the maximum signal strength for a given molecule at $TE = 0$ ms and infinite TR ([An and Lin, 2001](#)). Note that the factor $(1 - e^{-TR/T1})$ in the above equation is constant across compartments and approximately equal to 1. This is because even though $T1$ is likely to be much shorter in the vesicular compartment, the almost complete signal loss due to the short $T2$ at $TE > 35$ ms renders any $T1$ correction negligible when we consider percentage differences from baseline.

Therefore, the total predicted MRS signal for each metabolite S_T^α at time t , is given by:

$$\begin{aligned} S_T^\alpha(t) &= \sum_c S_c^\alpha(t) \\ &= \sum_c \Phi_c^\alpha(t) e^{-TE/T2_c^\alpha} \\ &= \Phi_0^\alpha \sum_c \mu_c^\alpha(t) e^{-TE/T2_c^\alpha} \end{aligned} \quad (20)$$

This predicted time-resolved signal is then averaged over the recording period δt to produce the observed MRS signal for each metabolite \hat{S}_T^α , which gives the observation equation:

$$\hat{S}_T^\alpha = \sum_c \langle \mu_c^\alpha(t) \rangle_{\delta t} e^{-TE/T2_c^\alpha} \quad (21)$$

where $\langle x \rangle_{\delta t}$ denotes the time average of x over the time window, δt . For simulation purposes in the present paper we have assumed $\Phi_0^\alpha = 1$.

In practice, as the cytosolic pool is so much larger than the ECS pool, changes in the MRS signal are driven almost exclusively by changes in the former. As an illustration, if 70% of the NT is initially in the cytosol, then 99.9% of the signal contribution is from the cytosolic and ECS compartments calculated using $TE = 30$ ms and $T2 = 5$ ms for the vesicular compartment. If vesicular $T2 = 10$ ms, this reduces to 97.5%, and for vesicular $T2 = 15$ ms, to 93.6%, with cytosolic/ECS $T2$ values taken from the literature (see Table 1). Subsequent movement of a portion of the NT pool from vesicles to other compartments will increase the signal in direct proportion to the quantity of NT released.

3.3. Simulations

We aim to study the response of a single fMRS voxel to the different stimulation types described previously, and will therefore consider the response of a single two-population model represented in Fig. 2. The following simulations were performed in MATLAB (The Mathworks Inc., MATLAB ver. R2019b) on a Dell PC using Intel(R) Core(TM) i7-7700HQ CPU 2.80 GHz with 32 GB RAM. The model was solved numerically using the forward Euler integration method with a time step of 0.01 ms, similar to (Kobayashi and Kitano, 2016). As an illustration, each graph relating to a specific stimulus types in Fig. 7 took approximately 35 mins to run.

3.3.1. Simulation 1 - Effect of firing rate and amplitude of firing on NT cycling dynamics

We varied the average firing rate (modelled as a series of Dirac functions) between 0 and 100 spikes s^{-1} and solved the differential equations governing NT cycling rates Eqs. (6) to (8) for 100 s. U was set to 0.7, as in (Tsodyks and Markram, 1997).

3.3.2. Simulation 2 - Effect of τ_r on vesicular refilling times

We set the average firing rate to 10 spikes s^{-1} and solved the differential equations governing NT cycling rates Eqs. (6) to (8) for 100 s while varying τ_r between 1000 and 5000 ms to determine the time course for the vesicular pool to reach its maximum steady state value of 30% of the total cortical Glu concentration (starting from fully depleted vesicles).

3.3.3. Simulation 3 - Effect of current stimulation on NT dynamics

We allow the MFM to run for 30 s to reach a steady-state and then apply either a positive (excitatory) or negative (inhibitory) tDCS input current for the remaining duration of the simulation (see coloured bars) set at $I_{ext}^E = \pm 2$ mA. Note that the data presented in Fig. 5 is for 10 s pre and post onset of stimulation. When presenting the temporal trace of the NT dynamics in Fig. 5, the activity is presented as an average over a sliding window of 1 s which is comparable to the time resolution of the MRS acquisitions (usually in the order of 1 to 5 seconds).

3.3.4. Simulation 4 - Effect of current stimulation on time-averaged NT dynamics

We applied a tDCS input current I_{ext}^E that was varied between -5 to +5 mA to the MFM. Initially, the model was allowed to run for 30 s to achieve a steady-state and then the input was applied for a further 30 s. In Fig. 6, the mean proportion of each of NT, GABA and Glu are presented for each of the pools, averaged over the duration of the simulation where the input current was applied.

3.3.5. Simulation 5 - Model predictions for pain, visual, and current stimulation

We applied an input current (modelled as defined for each case in 'Input Types') for I_{ext}^E varied between -5 to +5 mA (for the tDCS case, as before), and 0 to 10 mA (for vision and pain) to the MFM. In Fig. 7 initially, the model was allowed to run for 30 s to achieve a steady-state and then the input was applied for a further 30 s. The mean proportion of each NT, (GABA or Glu) within the ECS and cytosolic pools, averaged over the duration of the simulation where the input current was applied, are presented as a percentage of the total.

3.3.6. Simulation 6 - Calculation of change in MRS signal

We assigned different values for $T2$ relaxation constants for GABA and Glu based on whether the NT was found in the vesicles (invisible) or the ECS/cytosol (visible). For each of the input types described previously, we calculated a predicted MRS signal using the Observation model described previously (Eq. (21)). The total signal is calculated as a weighted sum of NT from each compartment with $T2$ values assumed as per Table 1, and using a typical echo time from empirical data. We plot this as a percentage difference from baseline (where $I_{ext}^E = 0$), see Fig. 7.

3.3.7. Simulation 7 - Effect of vesicular $T2$ and TE on model predictions

To assess the effect of the assumed value for vesicular $T2$ and TE on the model predictions, Simulation 6 was repeated for different combinations of these two parameters ($TE = 10, 50, 100$ ms; vesicular $T2 = 5, 10, 15$ ms), see Fig. 8.

3.4. Parameter values

All parameters have been set to values within their physiologically measurable ranges, where such values exist. Values in the model that are arbitrary or have been estimated include the connection strengths used in all simulations, and the $TE/T2$ values used in Simulation 6. For an analysis of the effects of these variables on model behaviour please see Results and Supplementary Information.

4. Results

In the present study, we investigated the effect of stimulation on neural activity and, in turn, on GABA and Glu dynamics. For this, we used the MFM described previously composed of 2 local networks, one excitatory and one inhibitory interconnected via AMPA and GABA receptor mediated synapses (see Fig. 2).

4.1. Effect of firing rate and amplitude of firing on NT cycling dynamics

In Fig. 3 the percentages of NT found in the R pool (vesicular, left), the X (ECS, middle), and the N pool (cytosolic, right) were averaged over the duration of the simulation and are presented as a function of firing rate. Additionally, the amplitude of the input signal was varied, which can be considered as a local measure of neural synchronisation in a MFM (Daffertshofer and van Wijk, 2011).

When firing rates are zero, the vesicular component is at its maximum (30% of the total) and as firing rates increase, this percentage reduces. Variations in amplitude either enhance or inhibit this effect.

Table 1

Parameter values used in the simulations unless stated otherwise in the text. T2 values for 'visible' compartments are standard values measured at 3 T. The parameters B and V_{\max} are normalised values.

Parameter	Definition	Values	Reference
C	membrane capacitance	0.01 F/m ²	(Pospischil et al., 2008)
g_L	leak membrane conductance	3 S/m ²	(Pospischil et al., 2008)
g_K^E, g_K^I	potassium membrane conductance	0.006 S/cm ² , 0.002 S/cm ²	(Pospischil et al., 2008)
g_{Na}^E, g_{Na}^I	sodium channel conductance	0.056 S/cm ² , 0.01 S/cm ²	(Pospischil et al., 2008)
V_0^E, V_0^I	adjust spike threshold	-58 mV, -68 mV	(Pospischil et al., 2008)
V_L^E, V_L^I	leak reversal potential	-70 mV, -56 mV	(Pospischil et al., 2008)
V_{Na}, V_K	Na/K reversal potential	50 mV, -90 mV	(Pospischil et al., 2008)
g_A, g_G	quantal conductance	25 nS, 10 nS	(Destexhe, 1997; Zou and Destexhe, 2007)
a^A, c^A	rate constants AMPA receptors	1.1 s ⁻¹ M ⁻¹ , 180 s ⁻¹	(Destexhe and Paré, 1999; Destexhe, 1997; Zou and Destexhe, 2007)
a^G, c^G	rate constants GABA receptors	5 ms ⁻¹ M ⁻¹ , 166 s ⁻¹	(Destexhe and Paré, 1999; Destexhe, 1997; Zou and Destexhe, 2007)
V_R^A, V_R^G	reversal potentials	0 mV, -80 mV	(Destexhe and Paré, 1999; Destexhe, 1997)
w_{EE}, w_{EI}, w_{IE}	coupling strengths	2	-
w_{II}	coupling strengths	0	-
U	fraction of NT released	0.01	(Tsodyks et al., 1998)
B	normalised value for concentration conversion	10 mM	-
N_0	lower bound preventing further vesicle packaging	0.7	est from (Kauppinen et al., 1994; Kauppinen and Williams, 1991; Pirttilä et al., 1993)
τ_x	rate constant	3 ms	(Tsodyks and Markram, 1997; Tsodyks et al., 1998)
τ_r	rate constant	1800 ms	(see Results)
$V_{\max}, V_{tr}, \sigma_V$	max firing rate, firing threshold	1.2 mV, 5 mV	(Destexhe et al., 1994)
T2 (Glu, visible), T2 (Glu, invisible)	T2 constant	181 ms, 5 ms	(Ganji et al., 2012), estimate
T2 (GABA, visible), T2 (GABA, invisible)	T2 constant	88 ms, 5 ms	(Edden et al., 2011), estimate
TE (Glu), TE (GABA)	echo time	30 ms, 68 ms	typical values used empirically
I_0^E	excitatory input current	5.3 mA	-

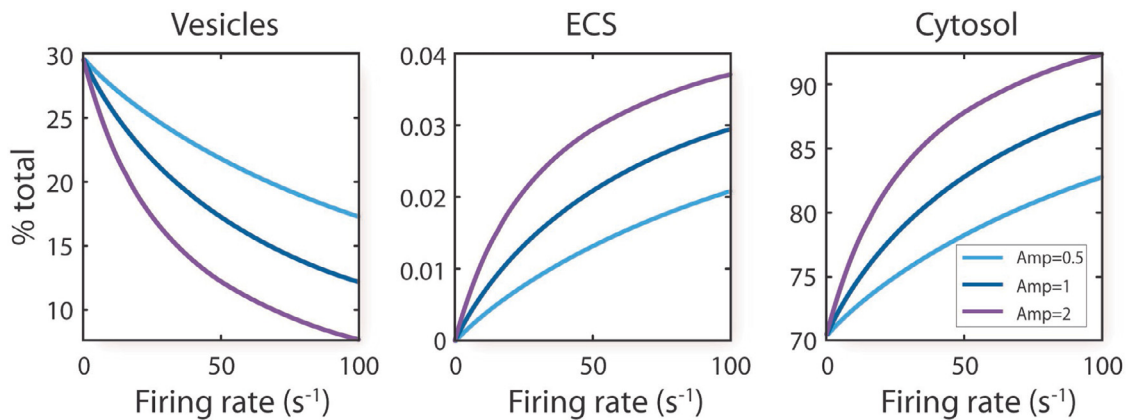


Fig. 3. Effect of firing rate and amplitude of firing on NT cycling dynamics The proportion of neurotransmitter (averaged over 100 s of simulation) found in the vesicular pool (left, R), the ECS (middle, X), and the cytosolic pool (right, N) is presented as a function of firing rate and neural synchrony (amplitude). As the firing rate increases, the NT concentration shifts from the vesicles to the ECS and cytosolic compartments. If vesicular NT is invisible to MRS then this would be reflected as an increase in the MRS signal. Additionally, the amplitude of the input signal was varied between 0.5 (light blue), 1 (dark blue) and 2 (purple); we found that increasing the amplitude enhanced the shift of NT from the vesicular to the ECS and cytosolic pools for the same firing rate whereas reducing the amplitude inhibited this effect.

We find that the reduction in vesicular NT is accompanied by an increased proportion of NT in the ECS (as a result of increased firing) or in the cytosol. The accumulation of NT in the cytosol is due to the mismatch between the rate that vesicles are depleted and the rate at which they are refilled, as observed in empirical data (Stevens and Tsujimoto, 1995). We observe that, in general, an increase in firing (or amplitude of firing) leads to a shift of NT from the vesicular pool to the ECS and cytosolic pools, whereas a decrease in firing (or am-

plitude) drives a shift of NT into the vesicles as predicted (also see Fig. 1).

4.2. Effect of τ_r on vesicular refilling times

Next, we examined the effect of τ_r on the refilling time of the vesicular pool to ensure that the model behaviour is physiologically plausible (see Fig. 4). τ_r governs the rate at which NT is recovered from the cytosol-

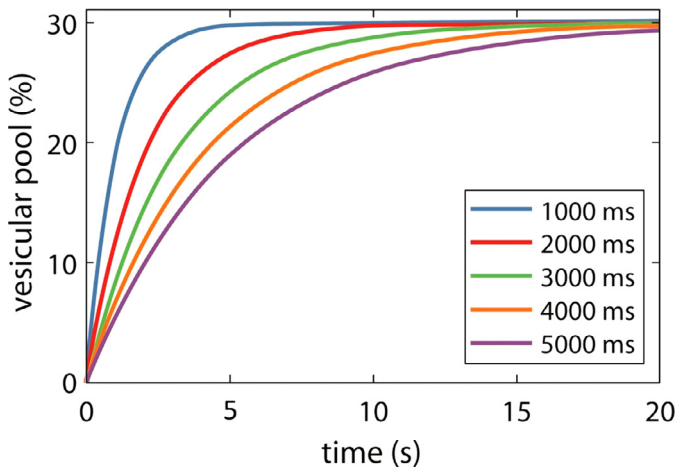


Fig. 4. Effect of τ_r on vesicle refilling times. The effect of τ_r on the refilling time of the vesicular pool. Here τ_r is varied between 1000 and 5000 ms and the time course of the vesicular pool to reach its steady state value (from empty) is shown. We fix the value of τ_r to be 1800 ms for the following simulations which results in refilling of the pool in approximately 10 seconds in line with (Stevens and Tsujimoto, 1995) using a firing rate of 10 spikes s^{-1} .

lic pool and packaged into vesicles ready for release. Here, τ_r is varied between 1000 and 5000 ms and the time course for the vesicular pool to reach its maximum steady state value of 30% of the total cortical Glu concentration (starting from fully depleted vesicles) is shown. We fix the value of τ_r to be 1800 ms for all simulations that follow as this value allows refilling of the vesicular pool in approximately 10 seconds which is in line with experimental data (Stevens and Tsujimoto, 1995)

using a firing rate of 10 spikes s^{-1} . We note that that the time taken to reduce this pool to a new lower steady-state value is in the order of 5 seconds, which is also in line with experimental data (Stevens and Tsujimoto, 1995), see Fig. 5.

4.3. Effect of current stimulation on NT dynamics

We interrogate the model with an current stimulation, analogous to tDCS, to make predictions about how the MFM activity affects NT dynamics. The temporal trace of the NT dynamics in each of the 3 pools (vesicular, ECS, cytosolic) is given for the E-population (orange, left column) and the I-population (blue, right), see Fig. 5.

For excitatory current input, in the case of the excitatory population, we observe a shift of Glu from the vesicles to the cytosolic pool. Under the assumption that NT in the vesicular pool does not contribute to the MRS signal, this would be reflected as an increased Glu MRS signal. In the case of the inhibitory population, we observe the opposite effect in that GABA starts to accumulate in the vesicles and is similarly reduced in the cytosolic compartment. This change would be reflected as a reduction in the GABA MRS signal.

Next, we applied an inhibitory current to the model after allowing the system to reach steady-state as described previously Fig. 5 (right panel). In this instance, we observe similar behaviour in both of the excitatory and inhibitory populations, specifically a shift of neurotransmitter from the cytosolic and ECS compartments to the vesicles. The effect of this in the spectroscopic data would be a reduction in both the Glu and GABA MRS signals.

Next, the model was used to systematically test the effects of current stimulation of varying polarity and magnitude on GABA and Glu dynamics. For excitatory input currents, we generally observe a shift of Glu from the vesicular to the cytosolic pools accompanied by a shift

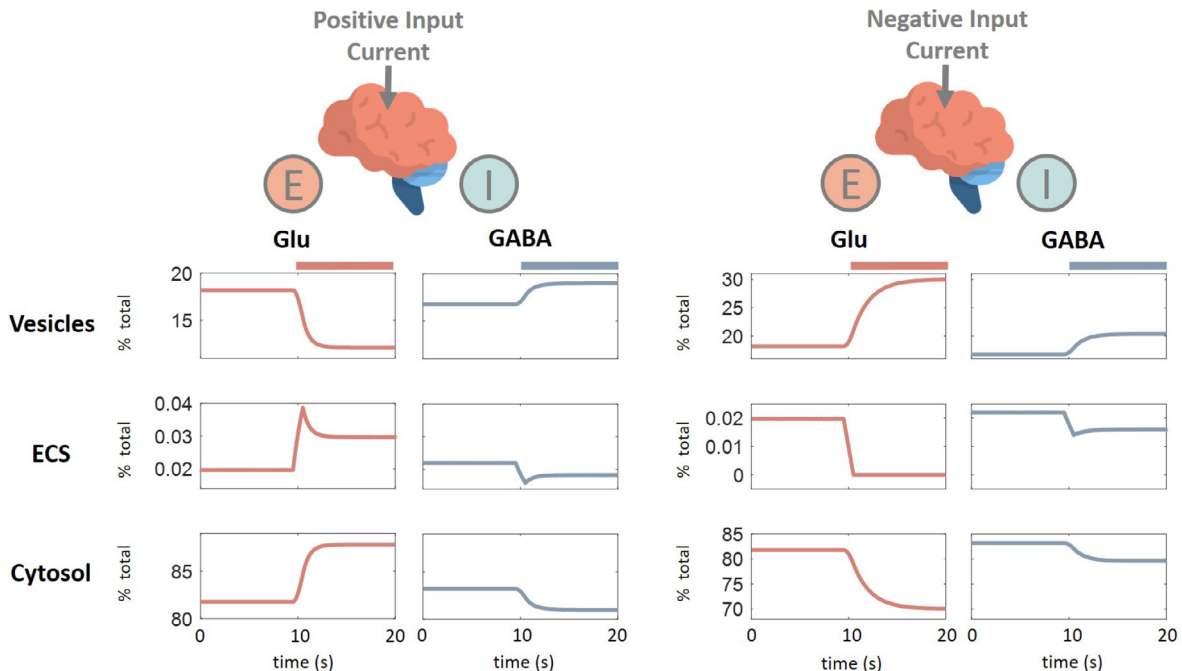


Fig. 5. Temporal dynamics of NT concentrations in response to polarity-specific current stimulation We assess the effect of applying an input current on the NT dynamics within each pool and describe the expected effect on the resulting MRS signal assuming that the vesicular compartment is MR-invisible. Left panels: the network is allowed to run for 30 seconds so as to reach steady-state and then the excitatory stimulus ($I_{ext}^E = 2$ mA) was applied for the remaining duration of the simulation (see coloured bars). In the case of the excitatory population (orange), we observe a shift of Glu from the vesicles to the cytosolic pool indicating an increased Glu MRS signal. In the case of the inhibitory population (blue), we observe the opposite effect in that GABA accumulates in the vesicles and is reduced in the cytosolic compartment. This would be reflected as a reduction in the GABA MRS signal in this condition. Note only 10 s of pre-stimulus activity is shown here. Right panels: an inhibitory current is applied in the same way ($I_{ext}^E = -2$ mA), causing the percentage of Glu and GABA in the vesicular pools to increase with a corresponding decrease in the cytosolic pool. The effect of this would be a reduction in both the Glu and GABA MRS signals.

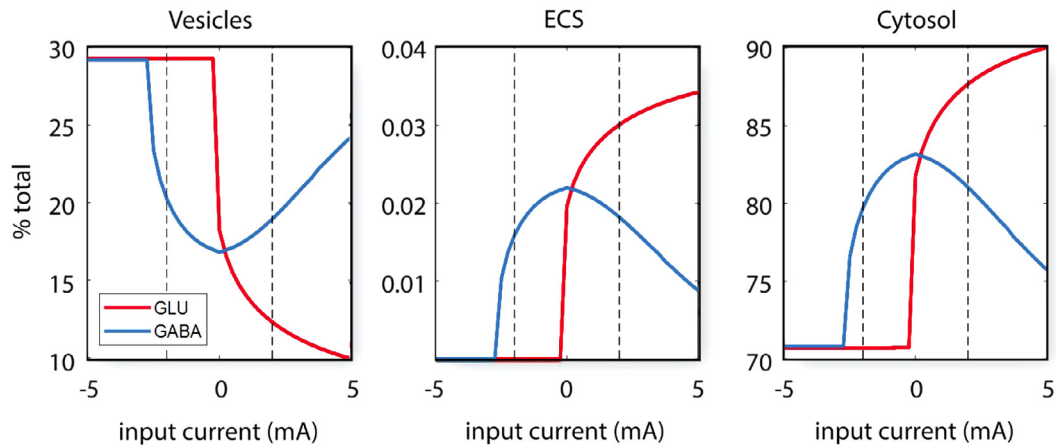


Fig. 6. Effect of polarity-specific current stimulation on mean NT concentrations in each pool We evaluate the proportion of Glu (red) and GABA (blue) in each of the three pools in response to current stimulation averaged over the 30 s of the simulation for a range of positive and negative currents. We note that the x-axis refers to the excitatory input current I_{ext}^E . Inhibitory (negative) current reduces GABA and Glu in the cytosolic pool, and increases them in the vesicles. Excitatory (positive) current reduces GABA and increases Glu in cytosolic pools, and has the opposite effect in the vesicles. The direction and magnitude of the change in the cytosol coincide with the direction and magnitude of change of the empirically measured GABA and Glu-MRS: inhibitory current reduces both neurotransmitters, while excitatory current decreases GABA and increases Glu. We conclude that the observed MRS concentrations and changes reflect the dynamics of the neurotransmitters within the cytosol and ECS, while their passage through the vesicles remains invisible to MR. Concentrations in the ECS appear negligible due to their rapid clearance rate. Vertical dashed lines indicate the specific current values of Fig. 5 ($I_{ext}^E = \pm 2$ mA).

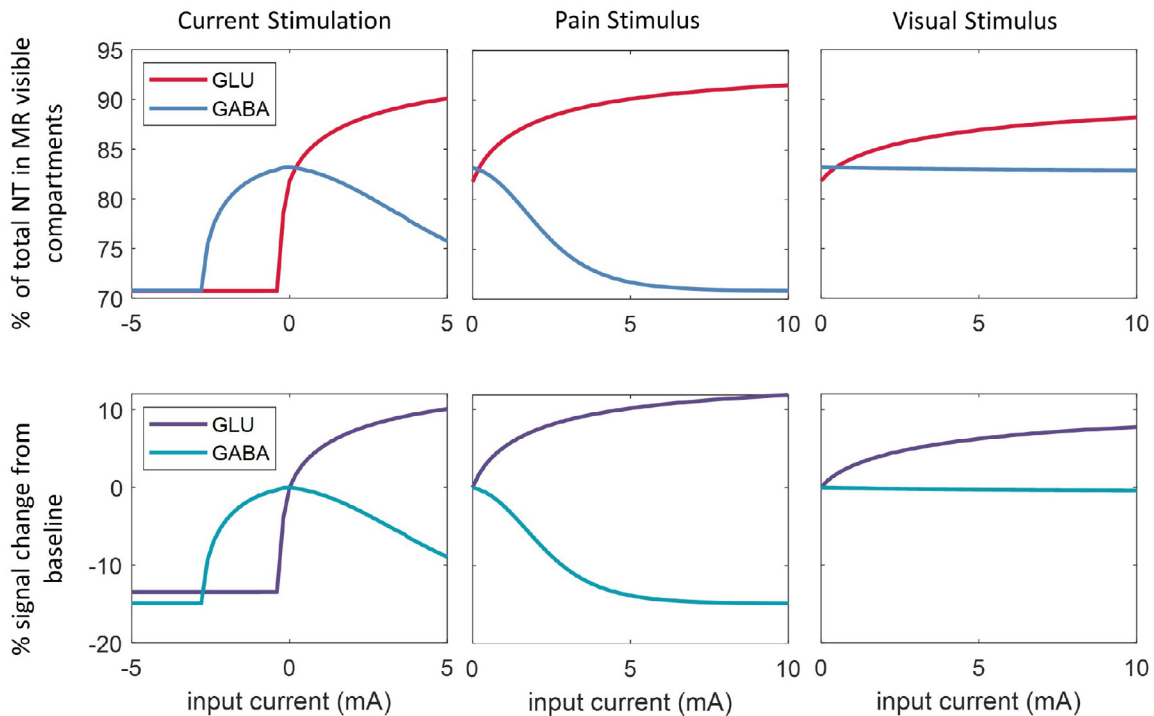


Fig. 7. Model predictions for pain, visual, and current stimulation We stimulate the model with the 3 input types: tDCS (left), Pain (middle), and Vision (right). Top panel: the percentage of total NT in the 'visible' pool (ECS and cytosol). Lower panel: we calculate the predicted MRS signal (S_T using the 'Observation Model') as a weighted sum of NT from each compartment. S_T is calculated using specific T2 values assigned to NT within each compartment with an assumed TE of 30 ms for Glu and 68 ms for GABA (see Table 1 for a list of all parameters). Results are expressed as a percentage difference from the baseline case, where $I_{ext}^e = 0$ mA. For sensory stimulation (pain and vision), we only consider input currents greater than 5 as that is the minimum input current required to elicit cell firing in this model.

of GABA from the cytosolic to the vesicular pool. Under our assumption that NT in the vesicular pool does not contribute to the MRS signal, the model predicts that we would observe a decrease in the GABA signal and an increase in the Glu MRS signal in experimental scenarios using excitatory current stimuli (anodal tDCS). For inhibitory currents, we observe a reduction in GABA and Glu in the ECS and cytosolic pools accompanied by an increase of NT in the vesicular pool compared to the baseline case ($I_{ext}^E = 0$ mA). Therefore, the model predicts that we would observe a reduction in the MRS sig-

nal for both GABA and Glu in experimental scenarios using inhibitory current stimuli (cathodal tDCS). Highlighted with dashed lines is the case where $I_{ext}^E \pm 2$ mA which corresponds to the diagrams shown in Fig. 5.

4.4. Model predictions for pain, visual, and current stimulation

We present the model predictions for 3 stimulus types: pain, visual, and current stimulation of varying intensities. In Fig. 7 top panel,

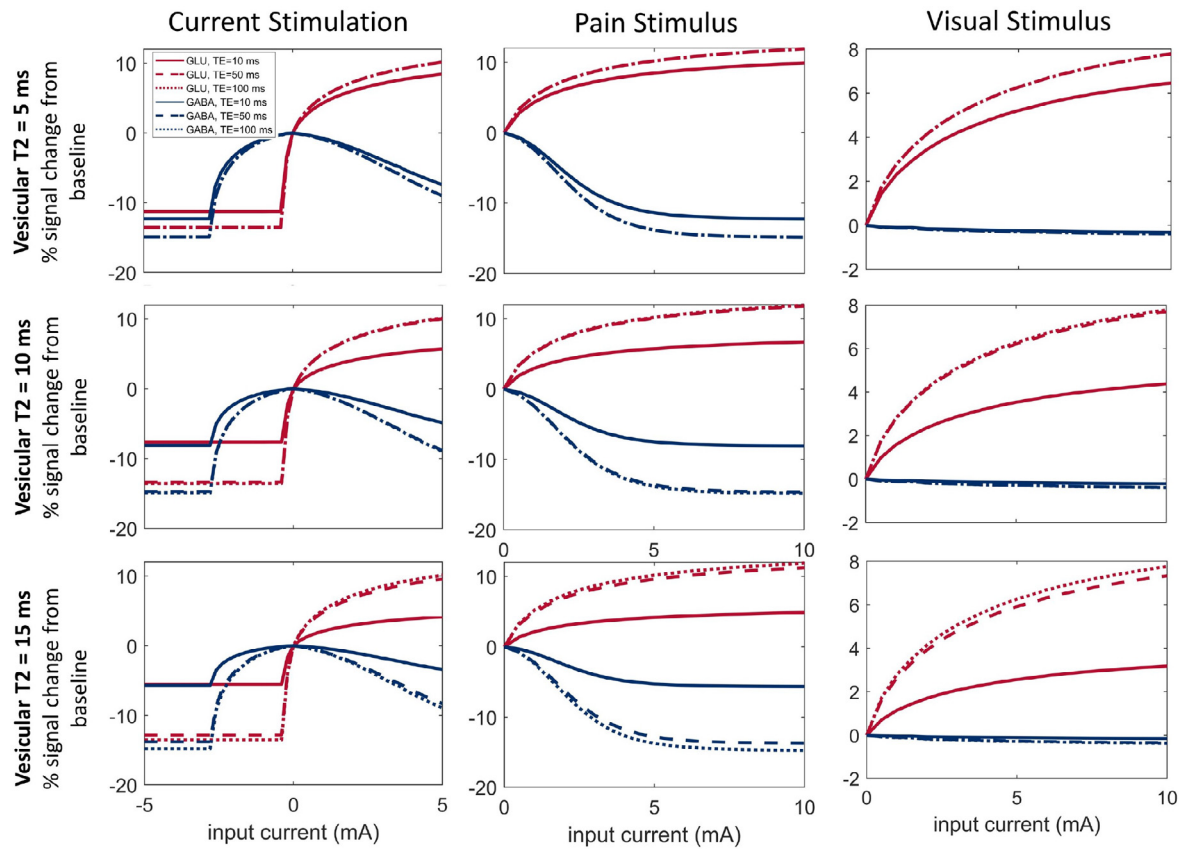


Fig. 8. Effect of vesicular T2 and TE We recreate Fig. 7 (lower panel) with different values for TE and assumed values for vesicular T2. Each column relates to the stimulation type, described as before: left, tDCS; middle, pain; right, visual. The top row assumes vesicular T2 to be 5 ms, the middle row 10 ms, and the lower row 15 ms. Echo times used are 10 ms (solid lines) and 50 (dashed lines), and 100 ms (dotted lines indistinguishable from TE=50 ms for vesicular T2 less than 15 ms).

we present the proportion of Glu (red) and GABA (blue) that is considered to be 'visible', i.e., the sum of the cytosolic and ECS compartments in response to the stimulation as a percentage of the total concentration. Pain and vision only allow for excitatory input currents and we observe that as the stimulus intensity increases, the proportion of visible Glu grows in both cases. We observe a greater reduction in GABA for the painful stimulus than for vision and this is due to the fact that the pain stimulus is modelled as targeting the inhibitory population directly whereas in the case of vision, the activity of the GABAergic cells is modulated indirectly via their connection to the excitatory population. In Fig. 7 lower panel, we calculate the predicted MRS signal intensity for each condition using the 'Observation Model' described previously and present this as a percentage difference from the baseline (when $I_{ext}^{\alpha} = 0$). We have assigned T2 values to NT within each compartment and assumed standard echo times from the literature (see Table 1). We observe that for approximately a 10% change in the proportion of visible Glu or GABA, we achieve a 12% signal increase. Please see Supplementary Information for a detailed exploration of the effect of assumed T2 values on these results.

4.5. Effect of vesicular T2 and TE

We present the variations in the model predictions for a range of assumed vesicular T2 (5, 10, and 15 ms) and TE (10, 50, and 100 ms) values for each of the stimulation types, essentially recreating Fig. 7 (lower panel). We find that for shorter echo times or longer assumed values for vesicular T2, the effect of compartmental redistribution on the MRS signal is diminished.

5. Discussion

In this study, we present a mathematical model that bridges between the physiological changes at the micro-scale of the cell and synapse and fMRS measurements of the neurotransmitters GABA and Glu at the macroscale. The results presented in this paper indicate that echo-time is an important timing parameter that can be leveraged to maximise fMRS experimental outcomes.

5.1. Comparison with empirical data

In the following section, we assess the model performance against empirical data in the literature. We focus on studies measuring changes in the concentration of GABA, Glu, or Glx using fMRS in healthy participants in response to either painful, visual, or tDCS stimuli. Within each section there is considerable variation in the findings reported. However, analysing emerging patterns from the findings is an important first step.

The original aim of the paper was to test how much of the signal could be explained by shifting of NT between compartments over short timescales of less than 1 min. Unfortunately, most studies use acquisition times longer than a minute and this is due to known issues with SNR in MRS measurements. The model provides predictions at a much faster spatial scale; a new steady-state is reached within 5 seconds in response to a change in activity levels. Further modelling, including kinetic modelling, will be required to explain longer-term changes in NT concentrations following stimulation, but here we provide a framework which offers a supplementary perspective to the purely metabolic one. With this in mind, we present a range of fMRS studies to compare with the model outputs.

Table 2

A summary of tDCS studies discussed in this section.

	System	Current	Glu/Glx change (%)	GABA change (%)	TE	Event-related/Block	Temporal Resolution
Anodal Stimulation							
(Bachtiar et al., 2015)	Motor	1 mA	not reported	reduction	68 ms (MEGA-PRESS)	Block	20 mins
(Clark et al., 2011)	Parietal lobe	2 mA	11%	not reported	40 ms	Block	30 mins
(Dwyer et al., 2019)	pSTG	2 mA	0%	0%	68 ms (MEGA-PRESS)	Block	10 mins
(Hunter et al., 2015)	Parietal lobe	2 mA	increase	not reported	40 ms	Block	30 mins
(Jalali et al. (2018))	Cerebellum	1.8 mA	0%	0%	68 ms (MEGA-PRESS)	Block	25 mins
(Kim S et al., 2014)	Motor	1.5 mA	0%	-19.77%	16 ms	Block	15 mins
(Stagg et al., 2009)	Motor	1 mA	0%	-9.2%	68 ms (MEGA-PRESS)	Block	10 mins
(Stagg et al., 2011)	Motor	1 mA	0%	-11.5%	68 ms (MEGA-PRESS)	Block	10 mins
Cathodal Stimulation							
(Kim S et al., 2014)	Motor	1.5 mA	0%	0%	16 ms	Block	15 mins
(Patel et al., 2019)	Motor	1 mA	not reported	-13.6%	68 ms (MEGA-PRESS)	Block	10 mins
(Stagg et al., 2009)	Motor	1 mA	-19.1%	-11.1%	68 ms (MEGA-PRESS)	Block	10 mins

5.1.1. Current stimulation - Empirical studies

Although tDCS studies are generally conducted over longer timescales than considered by the model, they are included here due to the fact that tDCS allows explicit negative/inhibitory stimulation to both neural populations simultaneously. We point out, however, that animal data indicates this to be a limitation of the measurement technologies, not the biology as neural changes occur rapidly, for example (Sánchez-León et al., 2021). This allows us to show that the same model responds differentially to stimulation and presents a more general and therefore more robust test to the origins of the fMRS signal.

MRS studies looking at the effect of current stimulation are summarised in Table 2. In response to anodal stimulation of between 1 and 2 mA, empirical studies indicated an increase in Glu of between 0 and 11% (model prediction 9% increase using 3 mA stimulus), and a decrease in GABA of between 0 and 19% (model prediction 5% reduction using 3 mA stimulus). Whereas, in response to cathodal stimulation of the same intensity, empirical studies indicated a decrease of Glu of between 0 and 19% (model prediction 14% reduction using 3 mA stimulus), and a decrease in GABA of between 0 and 13% (model prediction 15% reduction using 3 mA stimulus). We refer to a 3 mA input for comparison as this appears to match more closely the empirical results using 1–2 mA. Empirically measured changes are generally of greater magnitude than the model predictions, especially for GABA. This could be due to the fact that the duration of the experiments is much longer than the simulated data which represents 1 min of activity, meaning that contributions to the signal from other sources become more likely. tDCS is thought to modulate the excitability of targeted neural populations by altering membrane potential in a polarity specific way (Molaei-Ardekani et al., 2021). Anodal tDCS has generally been found to increase cortical excitability and cathodal tDCS to reduce it with these effects validated via TMS motor evoked potential amplitudes (Liebetanz et al., 2002). Excitatory current stimulation is thought to drive a reduction in the MRS GABA signal due to reduced activity of GAD-67 (Floyer-Lea et al., 2006; Stagg et al., 2009), which is an enzyme involved in GABA synthesis that reduces with increased excitatory firing (Hendry and Jones, 1988; Levy et al., 2002). The inclusion of these processes is beyond the scope of this work, although we note that even without these details, the model predictions are in line with empirical observations.

In the case of negative current stimulation, it has been suggested that Glu is reduced as a direct consequence of decreased neuronal firing

(Stagg et al., 2009), as Glu/Gln cycling is tightly linked to glucose oxidation and therefore, neural activity (Petroff et al., 2002; Rothman et al., 1999; Sibson et al., 1997, 1998). It has also been suggested that the reductions in GABA found during cathodal stimulation are explained due to the maintenance of the physiological balance between Glu, Gln, and GABA (see Martin and Tobin, 2000; Petroff, 2002; Sonnewald et al., 1993). In the model, this change is explained due to the reduction in inhibitory population firing activity although, in reality, this process is likely to be more complex. For example, in a recent study in the cat visual cortex, Zhao et al. found anodal (cathodal) tDCS enhanced (suppressed) the amplitude of visually evoked field potentials, these effects were not found in a sham condition (Zhao et al., 2020). The authors found anodal tDCS caused GABA to decrease with no change in Glu and cathodal tDCS to cause a reduction in Glu, but not GABA. Furthermore, the mechanism driving these changes was that the polarity of the tDCS selectively suppressed the expression of GABA- and glutamate-synthesizing enzymes.

5.1.2. Vision - Empirical studies

fMRS studies using visual stimulation are summarised in Table 3. In response to visual stimulation and using block designs, most empirical studies reported an increase in Glu of between 0 and 4% (model prediction up to 8% increase), with no change in GABA apart from a single study reporting a decrease of 5% (model prediction up to 1% decrease). A single event-related repetition suppression study saw modulation of Glu from -11% to +12%, and we note that this study used the longest echo time which would sensitise measurements to shifts of Glu between compartments. The model predictions are in line with these reports; the minimal inhibitory response of the model is because the effect of stimulation on inhibitory populations is an indirect effect of their connection to the activated excitatory population rather than via the stimulation itself. Essentially, we present the results from a 'block design' in our model with NT activity averaged over 30 s in response to a flickering stimulus. An 'event-related' design would yield larger changes as seen in the empirical studies (see the following section for a discussion of this).

5.1.3. Pain - Empirical studies

fMRS studies focussed on pain generally report the largest changes in metabolite concentrations and are presented in Table 4. In response to painful stimulation, empirical studies indicated an increase in Glu of

Table 3

A summary of the visual fMRS studies discussed in this section. Where there exists more than a single entry under 'temporal resolution', this indicates that data was presented at the higher temporal resolution but stats were calculated using averaged data over the longer timescale.

Authors	Glu/Glx change (%)	GABA change (%)	TE	Event-related/Block	Temporal Resolution
(Apšvalka et al., 2015)	+12/-11%	0%	105 ms	Event-related	36 s
(Bednařík et al., 2015)	3.3%	0%	26 ms	Block	2.7 mins/ 20 s
(Bednařík et al., 2017)	3.1–3.9%	0%	26 ms	Block	2.7 mins
(Boillat et al., 2020)	1.65%	0%	16 ms	Block	3 mins/ 1 min
(Ip et al., 2017)	2%	0%	36 ms	Block	64 s/ 16 s
(Lin et al., 2012)	2.5%	0%	6 ms	Block	6.6 mins
(Mangia et al., 2006)	3%	not reported	6 ms	Block	2 mins 40 s/ 20 s
(Mekle et al., 2017)	0%	-5%	6 ms	Block	10 mins 40 s/ 40 s
(Schaller et al., 2013)	4%	0%	6 ms	Block	3.3 mins/ 30 s

Table 4

A summary of the pain fMRS studies discussed in this section.

Authors	Glu/Glx change (%)	GABA change (%)	TE	Event-related/Block	Temporal Resolution
(Cleve et al., 2015)	21.5%	-15.1%	68 ms (MEGA-PRESS)	Event-related	3 s
(Cleve et al., 2015)	15.7%	-12.7%	68 ms (MEGA-PRESS)	Event-related	3 s
(Cleve et al., 2017)	0%	0%	68 ms (MEGA-PRESS)	Event-related	16 s
(de Matos et al., 2017)	0%	-10.8%	43 ms	Event-related	12 s
(Gussew et al., 2010)	18.1%	not reported	30 ms	Event-related	5 s
(Gutzeit et al., 2011)	16.4%	not reported	30 ms	Block	9 mins
(Gutzeit et al., 2013)	9%	not reported	30 ms	Block	3.48 mins
(Hansen et al., 2014)	0%	not reported	30 ms	Block	5 mins
(Kupers et al., 2009)	0%	15%	20 ms	Block	4 mins
(Mullins et al., 2005)	9.3%	not reported	20 ms	Block	10 mins

between 0 and 22% (model prediction up to 12% increase), and a general decrease in GABA of between 0 and 15% (model prediction up to 15% decrease). The model predictions are aligned with the general observation that increased pain correlates with increased Glu and reduced GABA. We note here that we implement a simplified model of acute pain in a single voxel which does not take into consideration top-down and bottom-up inputs as well as feedback loops which may account for disparities between the model predictions and empirical results, such as in (Kupers et al., 2009).

5.2. Block vs event-related study design

In its current form, the model predicts a greater change in NT dynamics for an event-related design rather than for a block design which aligns with empirical results. Event-related designs generally have a much finer temporal resolution than block designs and the signal is acquired very close to the stimulus onset. The model indicates that in just a few seconds the maximal change in NT is attained and therefore an event-related design will capture the full magnitude of the signal change as the data is only collected close to the stimulus onset. In a block design, it is usual that the stimulus is applied intermittently (flashing light, for example). In this case, the model returns to baseline during the inter-stimulus interval and the total signal is an average of the stimulus on and off periods which will dilute the magnitude of the signal change. The reason for this rapid return to baseline is that the model does not account for adaptation and plasticity mechanisms and understanding how these contribute to the NT signal change is an important area for future work.

5.3. Controversy in the fMRS literature

The model clearly predicts changes in NT for a wide variety of stimulus inputs and intensities, however, in reality, the outcomes are variable making it difficult to compare results. An important factor in this controversy is in the study design itself. For example, methodological differences such as sample size, stimulation parameters, variability in stimulating probe position, duration of stimulation, acquisition protocol, echo-time, MRS analysis method, reference metabolite, and brain

region, all contribute to the variability in the empirical data. Choice of echo time is particularly important as at short TE, MRS will be less sensitive to compartmental shifts of NT however, further work is required to determine the effect of this acquisition parameter on the fMRS signal. Ultimately, optimal scan acquisition will require balancing TE with constraints imposed by imaging system, brain region, SNR, and experimental paradigm.

5.4. Empirical support for model assumptions

In the model, we assume that there is no net increase in either Glu or GABA in the timescales shown here as it is assumed that flux through the Glu-Gln-GABA or TCA cycle would have minimal impact (Jelen et al., 2018; Mullins, 2018). However, we note that an alternative interpretation favours changes in metabolic flux as an explanation for stimulus-related Glu changes (Martínez-Maestro et al., 2019), based on calculations that the available pool of vesicular Glu is too small to account for the signal changes if this pool is released. We point out that this estimation is based on the assumption of 1 vesicle release per synapse at a single point in time (Barbour and Häusser, 1997). The model accounts for the sustained release of vesicular NT due to activation over many seconds driving the vesicular component closer to zero, or at least to a new lower steady-state value as firing rates increase. This has been found to be the case in as little as 5 seconds in animal studies using a preparation designed to mimic high frequency stimulation (Stevens and Tsujimoto, 1995). We suggest that in reality both of these processes contribute to the change in fMRS signal to different degrees depending on the temporal resolution of the experiment. This means that although the model was initially designed to explain short-term changes in physiology in response to stimulation, it may be that the same mechanisms presented here i.e., a mismatch between the rates of synthesis, repackaging, and exocytosis, also contribute to longer-term in vivo measurements in addition to changes in absolute concentrations brought about via de novo synthesis and degradation of GABA and Glu.

The key determinant of the shift of NT between the pools of differing MR visibility defined here, is the mismatch between the release and refilling rates of vesicles in response to an altered firing rate. Upon

sustained stimulation, the number of vesicles released per second has been found to reduce until a lower steady-state is reached (Stevens and Tsujimoto, 1995). The release rate is predicted to decline according to the equation $\frac{1}{(K_X+K_D)}$ where K_X is the rate of exocytosis, and K_D is the vesicular refilling rate (Stevens and Tsujimoto, 1995). In the same paper, the authors estimated K_X to be almost seven times greater than K_D . We chose τ_r to allow a vesicle refilling rate of approx 10 seconds as in (Stevens and Tsujimoto, 1995). Other authors have found this rate to be longer (23 seconds) (Hori and Takahashi, 2012). Similarly, the model was tuned to reach a new steady-state in response to stimulation after approx 5 seconds, as observed in animal data (Stevens and Tsujimoto, 1995). Further work is required to ascertain the direct effect of these rates on NT dynamics.

Animal work has shown that the average sustainable release capacity for a central synapse is approximately two vesicles per μm^3 per second (Danbolt, 2001). Assuming 5000 Glu molecules per vesicle (which is at the upper end of current estimations) (Danbolt, 2001), this equates to approximately 1 mMol min^{-1} which is equivalent to the 10% changes we observe in the model, assuming an average cortical Glu concentration of 10 mM (Danbolt, 2001; Schousboe, 1981). This rate would be further increased (allowing for even larger changes in shorter time scales) if not all cytosolic Glu were MRS-visible, as we have assumed here. This is higher than both the rate of flux through the Glu-Gln cycle (Shen et al., 1999) and the estimated rates of astrocytic uptake for Glu (Kanamori et al., 2002). We suggest that in the short term it is not a requirement for Glu production to keep up with metabolic demand as there is a surplus of Glu in the cytosol which can be recycled into vesicles. Astrocytic uptake rates must also be considered as a limiting factor; however, it has been argued that Glu uptake is relevant to the "slow component of glutamate removal [from the cleft]..." (Diamond and Jahr, 1997; Danbolt, 2001; Otis et al., 1996) and that immobilisation by binding is a much faster method of inactivating Glu, allowing some time for astrocytic uptake to take place. Therefore, in the short-term, these limiting factors may not apply.

5.5. Model limitations and future work

The metabolic pathway involving each of the neurotransmitters modelled here is highly complex; this holds in the case of Glu particularly. For example, within the neuron, cytosolic Glu may be utilised for new amino-acid synthesis, entry into the TCA cycle, or conversion into glutathione or GABA amongst many other possibilities (Mangia et al., 2012). Here we make the simplified assumption that all cytosolic Glu in the model is available for repackaging into vesicles for neurotransmission. For the purpose of the present work, we have assumed that cycling rates (time constants) of GABA and Glu are the same in the first approximation. Rigorously speaking, the molecular processes that underlie the metabolism of these NTs are distinct, which might lead to differences in their cycling rates. The current model does not account for processes involving Gln. Glu released at the synapse is almost entirely taken up by the surrounding glial cells and accumulates in the cytosol with a small fraction of released GABA. Approximately, 80% of astrocytic Glu is converted to Gln and is returned to the Glu-Gln(-GABA) cycle with the rest being degraded via the TCA cycle (Hertz and Rothman, 2017). The conversion rate of Gln from Glu appears to approximately match rates of conversion in the opposite direction (Hertz and Rothman, 2017). And so although there may be short-term transients, there are unlikely to be significant changes over the longer term. However, we note that various complexities such as the inhibition of this cycle due to large extracellular Glu/Gln concentrations (Hertz and Rothman, 2017), which may be the case after a period of activity, must also be accounted for. Future work will endeavour to consider all of these complexities.

We acknowledge that when considering concentration changes on minute time scales, rebalancing of steady-state TCA intermediates following metabolic stimulation and a degree of increased anaplerosis may

go some way to explaining neurotransmitter concentration changes. However, the goal of this paper was to explain much faster changes in a quantitative manner. Further work includes modelling of the anaplerotic pathway, including the malate-aspartate shuttle and the lactate astrocyte-neuron shuttle to examine the effect that these might have on MRS measurements over longer time scales (Mangia et al., 2009; Mason, 2017). Though metabolic consequences/effectors of activation do need to be considered, we also point out that, following (Sonnewald, 2014), 'as the TCA cycle cannot act as a carbon sink, anaplerosis must be coupled with cataplerosis', implying that net increases in Glu are unlikely to account for the increases found in fMRS studies.

Further work is required to substantiate the hypothesis that the vesicular pool of NT is not visible to MRS since there are no studies which we are aware of that have investigated MRS in vesicular preparations. There are studies of synaptosomes, which are nerve terminal preparations prepared by sub-cellular fractionation that contain membrane-sealed cytosol as well as synapses and vesicles (Petroff et al., 1992; Sonnewald and McKenna, 2002). However, the MRS was carried out on acid extracts of the preparations, thus destroying the integrity of vesicles. Furthermore, our assumption of an MR-invisible GABA pool is based on our knowledge of Glu, but as far as we are aware, this has not been established empirically.

The mean-field approximation used in this work, describes the evolution of the first-order moments of the system states (i.e. the means), and discarded higher order terms (Marreiros et al., 2009). A consequence of this first order approximation is that the model is unable to capture dependencies between the moments within or between the ensembles. As an example, the mean membrane potential of one population may be affected by the variance of the depolarisation of another or the same population (Deco et al., 2008). A possible future extension of this work might be to consider a second order approximation as in the dynamic mean-field framework, described in (Hasegawa, 2003).

This model is intended to replicate a generic patch of cortical sheet (or a standard MRS voxel) to understand how changes in neural activity (excitatory and inhibitory) might relate to observed changes in the fMRS signal. Future work should account for the anatomical diversity of different brain regions as well as the various types of interneurons and their cytoarchitecture. Tailoring the model to a specific neural region or circuit is an area for future work, as is the addition of plasticity mechanisms and adaptation as a major application of fMRS is in the study of plasticity. Another exciting avenue for future research will be to understand how the fMRS and BOLD signals are related in order to explain results found in simultaneous MRS-BOLD studies. To achieve this, the current model will be coupled to a haemodynamic response function which will allow the model to generate predictions for both imaging modalities.

6. Conclusions

In this paper, we bridge the gap between spatial scales by developing a mean-field model of macro measurements in fMRS, to test the validity of the hypothesis that fMRS reflects a shift of NT between pools. We have developed a mean-field model to link human in vivo quantification of task-related neurotransmitter changes via MRS to synaptic activity. We have shown that, using a biologically realistic model, it is possible to predict changes in GABA and Glu concentrations which are in agreement with experimentally observed values. We hope that this work highlights the issue of echo-time choice in fMRS experiments and how this important timing parameter can be leveraged to maximise experimental outcomes.

Data availability

Data will be made available on request.

Credit authorship contribution statement

Caroline A. Lea-Carnall: Conceptualization, Data curation, Formal analysis, Investigation, Methodology, Project administration, Software, Validation, Visualization, Writing – original draft, Writing – review & editing. **Wael El-Dereby:** Conceptualization, Investigation, Methodology, Supervision, Validation, Visualization, Writing – original draft, Writing – review & editing. **Charlotte J. Stagg:** Conceptualization, Investigation, Methodology, Supervision, Validation, Visualization, Writing – original draft, Writing – review & editing. **Stephen R. Williams:** Conceptualization, Investigation, Methodology, Supervision, Validation, Visualization, Writing – original draft, Writing – review & editing. **Nelson J. Trujillo-Barreto:** Conceptualization, Data curation, Formal analysis, Investigation, Methodology, Project administration, Supervision, Validation, Visualization, Writing – original draft, Writing – review & editing.

Acknowledgements

The authors would like to thank Prof. Peter Robinson for his careful reading and insightful comments on an early version of this manuscript, Daniel Wand for his assistance with graphics, and the anonymous reviewers for their invaluable insights which have improved the paper vastly. CLC is funded by the [Medical Research Council \(MRC\)](#) Grant MR/PO14445/1. WeD acknowledges ANID, Chile (projects FONDECYT 1201822, ANILLO ACT210053 and Basal FB0008), ValgrAI and the Generalitat Valenciana, Spain. NTB is funded by EPSRC Grant EP/N006771/1. CJS holds a Senior Research Fellowship, funded by the Wellcome Trust (224430/Z/21/Z). The Wellcome Centre for Integrative Neuroimaging is supported by core funding from the Wellcome Trust (203139/Z/16/Z).

Appendix A

A1. Spiking model equations

Here we include the standard equations for the gating variables of the Hodgkin-Huxley model described in the main paper. The time course of the voltage-mediated gating variables, which follow first-order kinetics, m, n, h for cell j belonging to population α where $\alpha \in \{E, I\}$ are given by:

$$\dot{m}_j^\alpha(t) = y_m(V_j^\alpha(t))(1 - m_j^\alpha(t)) - z_m(V_j^\alpha(t))m_j^\alpha(t) \quad (\text{A.1})$$

$$\dot{h}_j^\alpha(t) = y_h(V_j^\alpha(t))(1 - h_j^\alpha(t)) - z_h(V_j^\alpha(t))h_j^\alpha(t) \quad (\text{A.2})$$

$$\dot{n}_j^\alpha(t) = y_n(V_j^\alpha(t))(1 - n_j^\alpha(t)) - z_n(V_j^\alpha(t))n_j^\alpha(t) \quad (\text{A.3})$$

The activation and inactivation dynamics of each channel type, which can be described in terms of voltage-dependent transition rates x and y :

$$y_m(V_j^\alpha(t)) = \frac{-0.32(V_j^\alpha(t) - V_0^\alpha - 13)}{\exp[-(V_j^\alpha(t) - V_0^\alpha - 13)/4] - 1} \quad (\text{A.4})$$

$$z_m(V_j^\alpha(t)) = \frac{0.28(V_j^\alpha(t) - V_0^\alpha - 40)}{\exp[(V_j^\alpha(t) - V_0^\alpha - 40)/5] - 1} \quad (\text{A.5})$$

$$y_h(V_j^\alpha(t)) = 0.128 \exp[-(V_j^\alpha(t) - V_0^\alpha - 17)/18] \quad (\text{A.6})$$

$$z_h(V_j^\alpha(t)) = \frac{4}{1 + \exp[-(V_j^\alpha(t) - V_0^\alpha - 40)/5]} \quad (\text{A.7})$$

$$y_n(V_j^\alpha(t)) = \frac{-0.032(V_j^\alpha(t) - V_0^\alpha - 15)}{\exp[-(V_j^\alpha(t) - V_0^\alpha - 15)/5] - 1} \quad (\text{A.8})$$

$$z_n(V_j^\alpha(t)) = 0.5 \exp[-(V_j^\alpha(t) - V_0^\alpha - 10)/40] \quad (\text{A.9})$$

Where V_0^α for each cell-type is given in [Table 1](#), all taken from ([Pospischil et al., 2008](#)).

A2. Derivation of the mean-field model

In the spiking neuron model previously described, the input to a postsynaptic cell is determined by the Glu (excitatory) or GABA (inhibitory) concentration found instantaneously in the cleft. For each conductance, j , this is calculated using the compartmental model described in [Section 2.1.2](#). As described in the text, the input to that model is defined by the train of spikes from all connected presynaptic neurons. The firing rate from each source population k is calculated as a Heaviside function (H) on $(V_k - V_{tr})$, which determines the proportion of cells firing by comparing their membrane potential to the threshold V_{tr} . Using mean-field theory, the input to the compartmental model at a given time point can be expressed as the expected value of the membrane potential over the afferent population of neurons [Eq. \(A.10\)](#). Under the Laplace approximation the distribution of the membrane potential is assumed to be Gaussian and therefore the integral in [Eq. \(A.10\)](#) reduces to the cumulative distribution function of the Gaussian distribution ([Marreiros et al., 2009](#); [Wilson and Cowan, 1972](#); [Zandt et al., 2014](#)).

$$\begin{aligned} \zeta_j &= \int q(V^{(k)})H(V^{(k)} - V_{tr})dV^{(k)} \\ &= S(\mu_V^{(k)} - V_{tr}, \sigma_V^{(k)}) \end{aligned} \quad (\text{A.10})$$

Where S denotes the cumulative distribution function of the membrane's depolarisation (or its deviation from resting levels), and $q(V^{(k)})$ is the Gaussian distribution of the membrane potential with mean $\mu_V^{(k)}$ and standard deviation $\sigma_V^{(k)}$.

Following ([Marreiros et al., 2009](#)), the cumulative distribution function S in [Eq. \(A.10\)](#) can be approximated using the sigmoid function [Eq. \(A.11\)](#) which converts the mean membrane potential for the population to a fractional firing rate ([Wilson and Cowan, 1972, 1973](#); [Zandt et al., 2014](#)), V_{tr} defines the point at which the function is half-activated and σ_V sets the steepness of the curve:

$$S(\mu_V, \sigma_V) = \frac{V_{max}}{1 + \exp((V_{tr} - \mu_V^{(k)}(t))/\sigma_V^{(k)})} \quad (\text{A.11})$$

Using these expressions, the input to the compartmental model after averaging over the afferents from the population of a given type, can be expressed by replacing the spike trains in equations [Eqs. \(6\)](#) to [\(7\)](#) with the sigmoid function given in [Eq. \(A.10\)](#) to give (similarly to [Tsodyks et al., 1998](#)):

$$\dot{R}_j^\alpha(t) = -\frac{f(N_j^\alpha(t) - N_0)}{\tau_r} - UR_j^\alpha(t)S(\mu_V^\alpha(t), \sigma_V) \quad (\text{A.12})$$

$$\dot{X}_j^\alpha(t) = -\frac{X_j^\alpha(t)}{\tau_x} + UR_j^\alpha(t)S(\mu_V^\alpha(t), \sigma_V) \quad (\text{A.13})$$

To estimate the network statistics, we approximate the dynamical equations for the statistical moments of the networks state variables. First, we define the vector x_p of the model variables for each population α as $x_p^\alpha = [x_1^\alpha, x_2^\alpha, \dots, x_n^\alpha] = [V^E, n^E, m^E, h^E, \dots]$ for a local population of neurons. We express the system of stochastic differential equations $f(x)$ defined as [Eqs. \(1\)](#) to [\(7\)](#) in terms of the first-order moments (the mean) of the distribution of the states, represented by the vector μ_p^α .

We define

$$\mu_p^\alpha(t) = \langle x_p^\alpha(t) \rangle \quad (\text{A.14})$$

State variables are expressed as deviations from the means

$$x_p^\alpha(t) = \mu_p^\alpha(t) + \delta x_p(t) \quad (\text{A.15})$$

Performing a first-order Taylor expansion of $h(x)$ around the mean $x = \mu$ we get (i.e., ignoring all second-order and higher terms):

$$h(x) = h(\mu) + \sum_p \frac{\partial h}{\partial x_p}(\mu) \cdot \delta x_p \quad (\text{A.16})$$

Averaging over realisations and noting that:

$$\langle \delta x_p(t) \rangle = 0 \quad (\text{A.17})$$

We obtain the motion equations for the means of the state variables for a local area p given as:

$$C\dot{\mu}_V^\alpha(t) = I_{int}^\alpha(t) - I_{ext}^\alpha(t) - w_{Ea}I_A^\alpha(t) - w_{Ia}I_G^\alpha(t) - I_0^\alpha \quad (\text{A.18})$$

$$I_{int}^\alpha(t) = -g_L(\mu_V^\alpha(t) - V_L^\alpha) - g_{Na}^\alpha\mu_m^{\alpha 3}(t)\mu_h^\alpha(t)(\mu_V^\alpha(t) - V_{Na}^\alpha) - g_K^\alpha\mu_n^{\alpha 4}(t)(\mu_V^\alpha(t) - V_K^\alpha) \quad (\text{A.19})$$

$$I_A^\alpha(t) = g_A(\mu_V^\alpha(t) - V_R^A)\mu_p^A(t) \quad (\text{A.20})$$

$$I_G^\alpha(t) = g_G(\mu_V^\alpha(t) - V_R^G)\mu_p^G(t) \quad (\text{A.21})$$

$$\dot{\mu}_R^\alpha(t) = \frac{f(\mu_N^\alpha(t) - N_0)}{\tau_r} - U\mu_R^\alpha(t)S(\mu_V^\alpha(t), \sigma_V) \quad (\text{A.22})$$

$$\dot{\mu}_X^\alpha(t) = -\frac{\mu_X^\alpha(t)}{\tau_x} + U\mu_R^\alpha(t)S(\mu_V^\alpha(t), \sigma_V) \quad (\text{A.23})$$

$$S(\mu_V^\alpha, \sigma_V) = \frac{V_{max}}{1 + \exp((V_{tr} - \mu_V^\alpha(t))/\sigma_V)} \quad (\text{A.24})$$

$$\dot{\mu}_p^\beta(t) = a^\beta b^\beta(t)(1 - \mu_p^\beta(t)) - c^\beta \mu_p^\beta(t) \quad (\text{A.25})$$

$$\dot{\mu}_m^\alpha(t) = y_m(\mu_V^\alpha(t))(1 - \mu_m^\alpha(t)) - z_m(\mu_V^\alpha(t))\mu_m^\alpha(t) \quad (\text{A.26})$$

$$\dot{\mu}_n^\alpha(t) = y_n(\mu_V^\alpha(t))(1 - \mu_n^\alpha(t)) - z_n(\mu_V^\alpha(t))\mu_n^\alpha(t) \quad (\text{A.27})$$

$$\dot{\mu}_h^\alpha(t) = y_h(\mu_V^\alpha(t))(1 - \mu_h^\alpha(t)) - z_h(\mu_V^\alpha(t))\mu_h^\alpha(t) \quad (\text{A.28})$$

Please refer to Section 2.2 for a description of the parameters.

Supplementary material

Supplementary material associated with this article can be found, in the online version, at [10.1016/j.neuroimage.2022.119813](https://doi.org/10.1016/j.neuroimage.2022.119813)

References

- Abbott, L.F., Chance, F.S., 1995. Drivers and modulators from push-pull and balanced synaptic input. *Prog Brain Res* 149, 147–155. doi:[10.1016/S0079-6123\(05\)49011-1](https://doi.org/10.1016/S0079-6123(05)49011-1).
- An, H., Lin, W., 2001. Spin Density, T_1 , T_2 , T_2^* Relaxation and Bloch Equations. *Current Protocols in Magnetic Resonance Imaging* 00, B3.1.1–B3.1.10. <https://doi.org/10.1002/0471142719.mib0301s00>.
- Apšvalka, D., Gadie, A., Clemence, M., Mullins, P.G., 2015. Event-related dynamics of glutamate and BOLD effects measured using functional magnetic resonance spectroscopy (fMRS) at 3T in a repetition suppression paradigm. *Neuroimage* 118, 292–300. doi:[10.1016/j.neuroimage.2015.06.015](https://doi.org/10.1016/j.neuroimage.2015.06.015).
- Bachtari, V., Near, J., Johansen-Berg, H., Stagg, C.J., 2015. Modulation of GABA and resting state functional connectivity by transcranial direct current stimulation. *eLife* 4, e08789. doi:[10.7554/eLife.08789](https://doi.org/10.7554/eLife.08789).
- Barbour, B., Häusser, M., 1997 Sep. Intersynaptic diffusion of neurotransmitter. *Trends in Neurosciences* 20 (9), 377–384. doi:[10.1016/S0166-2236\(96\)20050-5](https://doi.org/10.1016/S0166-2236(96)20050-5).
- Bartos, M., Vida, I., Jonas, P., 2007. Synaptic mechanisms of synchronized gamma oscillations in inhibitory interneuron networks. *Nat Rev Neurosci* 8, 45–56. doi:[10.1038/nrn2044](https://doi.org/10.1038/nrn2044).
- Bednařík, P., Tkáč, I., Giove, F., DiNuzzo, M., Deelchand, D.K., Emir, U.E., Eberly, L.E., Mangia, S., 2015. Neurochemical and BOLD responses during neuronal activation measured in the human visual cortex at 7 Tesla. *J Cereb Blood Flow Metab* 35 (4), 601–610. doi:[10.1038/jcbfm.2014.233](https://doi.org/10.1038/jcbfm.2014.233).
- Bednařík, P., Tkáč, I., Giove, F., Eberly, L.E., Deelchand, D.K., Barreto, F.R., Mangia, S., 2017. Neurochemical responses to chromatic and achromatic stimuli in the human visual cortex. *J Cereb. Blood Flow Metab* 38 (2), 347–359. doi:[10.1177/0271678X17695291](https://doi.org/10.1177/0271678X17695291).
- Berzhanskaya, J., Chernyy, N., Gluckman, B., Schiff, S., Ascoli, G., 2013. Modulation of hippocampal rhythms by subthreshold electric fields and network topology. *J. Comput. Neurosci* 34 (3), 369–389. doi:[10.1007/s10827-012-0426-4](https://doi.org/10.1007/s10827-012-0426-4).
- Bloch, F., 1946. Nuclear induction. *Phys. Rev* 70, 460–474. doi:[10.1103/PhysRev.70.460](https://doi.org/10.1103/PhysRev.70.460).
- Boillat, Y., Xin, L., van der Zwaag, W., Gruetter, R., 2020. Metabolite concentration changes associated with positive and negative BOLD responses in the human visual cortex: a functional MRS study at 7 Tesla. *J. Cereb. Blood Flow Metab* 40 (3), 488–500. doi:[10.1177/0271678X19831022](https://doi.org/10.1177/0271678X19831022).

- Bonaiuto, J., Bestmann, S., 2015. Chapter 4 - understanding the nonlinear physiological and behavioral effects of tDCS through computational neurostimulation. *Prog. Brain Res* 222, 75–103. doi:[10.1016/bs.pbr.2015.06.013](https://doi.org/10.1016/bs.pbr.2015.06.013).
- Bustillo, J., Rowland, L., Mullins, P., Jung, R., Chen, H., Qualls, C., Hammond, R., Brooks, W., Lauriello, J., 2010. 1H-MRS At 4 Tesla in minimally treated early schizophrenia. *Mol. Psychiatry* 15 (6), 629–636. doi:[10.1038/mp.2009.121](https://doi.org/10.1038/mp.2009.121).
- Clark, V.P., Coffman, B.A., Trumbo, M.C., Gasparovic, C., 2011. Transcranial direct current stimulation (tDCS) produces localized and specific alterations in neurochemistry: a 1H magnetic resonance spectroscopy study. *Neurosci. Lett* 500 (1), 67–71. doi:[10.1016/j.neulet.2011.05.244](https://doi.org/10.1016/j.neulet.2011.05.244).
- Cleve, M., Gussew, A., Reichenbach, J.R., 2015. In vivo detection of acute pain-induced changes of GABA+ and Glx in the human brain by using functional 1H MEGA-PRESS MR spectroscopy. *Neuroimage* 105, 67–75. doi:[10.1016/j.neuroimage.2014.10.042](https://doi.org/10.1016/j.neuroimage.2014.10.042).
- Cleve, M., Gussew, A., Wagner, G., Bär, K.J., Reichenbach, J.R., 2017. Assessment of intra- and inter-regional interrelations between GABA+, Glx and BOLD during pain perception in the human brain - A combined 1H fMRS and fMRI study. *Neuroscience* 365, 125–136. doi:[10.1016/j.neuroscience.2017.09.037](https://doi.org/10.1016/j.neuroscience.2017.09.037).
- Czeiger, D., White, E.L., 1993. Synapses of extrinsic and intrinsic origin made by callosal projection neurons in mouse visual cortex. *J. Comp. Neurol* 330 (4), 502–513. doi:[10.1002/cne.903300406](https://doi.org/10.1002/cne.903300406).
- Daffertshofer, A., van Wijk, B.C., 2011. On the influence of amplitude on the connectivity between phases. *Front. Neuroinform* 5, 6. doi:[10.3389/fninf.2011.00006](https://doi.org/10.3389/fninf.2011.00006).
- Danbolt, N.C., 2001. Glutamate uptake. *Prog. Neurobiol* 65 (1), 1–105. doi:[10.1016/S0304-0082\(00\)00067-8](https://doi.org/10.1016/S0304-0082(00)00067-8).
- de Matos, N.M.P., Hock, A., Wyss, M., Ettlin, D.A., Brügger, M., 2017. Neurochemical dynamics of acute orofacial pain in the human trigeminal brainstem nuclear complex. *Neuroimage* 162, 162–172. doi:[10.1016/j.neuroimage.2017.08.078](https://doi.org/10.1016/j.neuroimage.2017.08.078).
- Deco, G., Jirsa, V.K., Robinson, P.A., Breakspear, M., Friston, K., 2008. The Dynamic Brain: From Spiking Neurons to Neural Masses and Cortical Fields. *PLoS Comput Biol* 4 (8), e1000092. doi:[10.1371/journal.pcbi.1000092](https://doi.org/10.1371/journal.pcbi.1000092).
- Deco, G., Ponce-Alvarez, A., Hagmann, P., Romani, G.L., Mantini, D., Corbetta, M., 2014. How local excitation inhibition ratio impacts the whole brain dynamics. *J. Neurosci* 34 (23), 7886–7898. doi:[10.1523/JNEUROSCI.5068-13.2014](https://doi.org/10.1523/JNEUROSCI.5068-13.2014).
- Destexhe, A., Paré, D., 1999. Impact of network activity on the integrative properties of neocortical pyramidal neurons in vivo. *J Neurophysiol* 81 (4), 1531–1547. doi:[10.1152/jn.1999.81.4.1531](https://doi.org/10.1152/jn.1999.81.4.1531).
- Destexhe, A., Mainen, Z.F., Sejnowski, T.J., 1994. Synthesis of models for excitable membranes, synaptic transmission and neuromodulation using a common kinetic formalism. *J. Comp. Neurosci* 1 (3), 195–230. doi:[10.1007/BF00961734](https://doi.org/10.1007/BF00961734).
- Destexhe, A., 1997. Kinetic Models of Synaptic Transmission. In: Koch, C., Segev, I., Mainen, Z.F., Senowski, T.J. (Eds.), 2nd Edition, *Methods in Neural Modeling*. MIT Press, Cambridge MA.
- Diamond, J., Jahr, C., 1997. Transporters buffer synaptically released glutamate on a submillisecond time scale. *The J neurosci* 17, 4672–4687. doi:[10.1523/JNEUROSCI.17-12-04672.1997](https://doi.org/10.1523/JNEUROSCI.17-12-04672.1997).
- Dwyer, G.E., Craven, A.R., Kompus, K., Assmus, J., Erslund, L., Hugdahl, K., Grüner, R., 2019. No effects of anodal tDCS on local GABA and Glx levels in the left posterior superior temporal gyrus. *Front. Neurol* 9. doi:[10.3389/fneur.2018.01145](https://doi.org/10.3389/fneur.2018.01145).
- Edden, R.A.E., Intrapirromkul, J., Zhu, H., Cheng, Y., Barker, P.B., 2011. Measuring T2 in vivo with J-difference editing: application to GABA at 3 Tesla. *J. Magn. Reson. Imaging* 35 (1), 229–234. doi:[10.1002/jmri.22865](https://doi.org/10.1002/jmri.22865).
- Elhanany, E., White, E.L., 1990. Intrinsic circuitry: synapses involving the local axon collaterals of corticocortical projection neurons in the mouse primary somatosensory cortex. *J. Comp. Neurol* 291 (1), 43–54. doi:[10.1002/cne.902910105](https://doi.org/10.1002/cne.902910105).
- Floyer-Lea, A., Wylezinska, M., Kincses, T., Matthews, P.M., 2006. Rapid modulation of GABA concentration in human sensorimotor cortex during motor learning. *J. Neurophysiol* 95 (3), 1639–1644. doi:[10.1152/jn.00346.2005](https://doi.org/10.1152/jn.00346.2005).
- Freund, T.F., Katona, I., 2007. Perisomatic inhibition. *Neuron* 56 (1), 33–42. doi:[10.1016/j.neuron.2007.09.012](https://doi.org/10.1016/j.neuron.2007.09.012).
- Ganji, S.K., Banerjee, A., Patel, A.M., Zhao, Y.D., Dimitrov, I.E., Browning, J.D., Brown, E.S., Maher, E.A., Choi, C., 2012. T2 Measurement of J-coupled metabolites in the human brain at 3T. *NMR Biomed* 25 (4), 523–529. doi:[10.1002/nbm.1767](https://doi.org/10.1002/nbm.1767).
- Gussew, A., Rzanny, R., Erdtel, M., Scholle, H.C., Kaiser, W.A., Mentzel, H.J., Reichenbach, J.R., 2010. Time-resolved functional 1H MR spectroscopic detection of glutamate concentration changes in the brain during acute heat pain stimulation. *Neuroimage* 49 (2), 1895–1902. doi:[10.1016/j.neuroimage.2009.09.007](https://doi.org/10.1016/j.neuroimage.2009.09.007).
- Gutzeit, A., Meier, D., Meier, M.L., von Weymarn, C., Ettlin, D.A., Graf, N., Froehlich, J.M., Binkert, C.A., Brügger, M., 2011. Insula-specific responses induced by dental pain. A proton magnetic resonance spectroscopy study. *Eur Radiol* 21 (4), 807–815. doi:[10.1007/s00330-010-1971-8](https://doi.org/10.1007/s00330-010-1971-8).
- Gutzeit, A., Meier, D., Froehlich, J.M., Hergan, K., Kos, S., Weymarn, C. V., Lutz, K., Ettlin, D., Binkert, C.A., Mutschler, J., Sartoretto-Schefer, S., Brügger, M., 2013. Differential NMR spectroscopy reactions of anterior/posterior and right/left insular subdivisions due to acute dental pain. *Eur. Radiol* 23 (2), 450–460. doi:[10.1007/s00330-012-2621-0](https://doi.org/10.1007/s00330-012-2621-0).
- Hansen, T.M., Olesen, A.E., Simonsen, C.W., Drewes, A.M., Frøkjær, J.B., 2014. Cingulate metabolites during pain and morphine treatment as assessed by magnetic resonance spectroscopy. *J. Pain Res* 7, 269–276. doi:[10.2147/JPR.S61193](https://doi.org/10.2147/JPR.S61193).
- Hasegawa, H., 2003. Dynamical mean-field theory of noisy spiking neuron ensembles: application to the Hodgkin-Huxley model. *Phys. Rev. E* 68 (4 Pt 1), 041909. doi:[10.1103/PhysRevE.68.041909](https://doi.org/10.1103/PhysRevE.68.041909).
- Hendry, S.H., Jones, E.G., 1988. Activity-dependent regulation of GABA expression in the visual cortex of adult monkeys. *Neuron* 1 (8), 701–712. doi:[10.1016/0896-6273\(88\)90169-9](https://doi.org/10.1016/0896-6273(88)90169-9).
- Hertz, L., Rothman, D.L., 2017. Glutamine-glutamate cycle flux is similar in cultured astrocytes and brain and both glutamate production and oxidation are mainly cat-

- alyzed by aspartate aminotransferase. *Biology (Basel)* 6 (1):17. doi:10.3390/biology6010017.
- Hodgkin, A.L., Huxley, A.F., 1952. A quantitative description of membrane current and its application to conduction and excitation in nerve. *J. Physiol. (Lond.)* 117, 500–544. doi:10.1113/jphysiol.1952.sp004764.
- Hori, T., Takahashi, T., 2012. Kinetics of synaptic vesicle refilling with neurotransmitter glutamate. *Neuron* 76 (3), 511–517. doi:10.1016/j.neuron.2012.08.013.
- Hunter, MA, Coffman, BA, Gasparovic, C, Calhoun, VD, Trumbo, MC, Clark, VP, 2015. Baseline effects of transcranial direct current stimulation on glutamatergic neurotransmission and large-scale network connectivity. *Brain Res* 1594, 92–107. doi:10.1016/j.brainres.2014.09.066.
- Hyder, F., Herman, P., Bailey, C.J., Möller, A., Globinsky, R., Fulbright, R.K., Rothman, D.L., Gjedde, A., 2016. Uniform distributions of glucose oxidation and oxygen extraction in gray matter of normal human brain: no evidence of regional differences of aerobic glycolysis. *J. Cereb. Blood Flow Metab.* 36, 903–916. doi:10.1177/0271678X15625349.
- Ip, L.B., Berrington, A., Hess, A.T., Parker, A.J., Emir, U.E., Bridge, H., 2017. Combined fMRI-MRS acquires simultaneous glutamate and BOLD-fMRI signals in the human brain. *Neuroimage* 155, 113–119. doi:10.1016/j.neuroimage.2017.04.030.
- Jalali, R., Chowdhury, A., Wilson, M., Miall, R., Galea, J., 2018. Neural changes associated with cerebellar tDCS studied using MR spectroscopy. *Exp. Brain Res.* 236 (4), 997–1006. doi:10.1007/s00221-018-5170-1.
- Jelen, L.A., King, S., Mullins, P.G., Stone, J.M., 2018. Beyond static measures: a review of functional magnetic resonance spectroscopy and its potential to investigate dynamic glutamatergic abnormalities in schizophrenia. *J. Psychopharm.* 32 (5), 497–508. doi:10.1177/0269881117747579.
- Johnson, R.R., Burkhalter, A., 1996. Microcircuitry of forward and feedback connections within rat visual cortex. *J. Comp. Neurol.* 368 (3), 383–398. doi: 10.1002/(SICI)1096-9861(19960506)368:3<383::AID-CNE5>3.0.CO;2-1.
- Kanamori, K., Ross, B.D., Kondrat, R.W., 2002. Glial uptake of neurotransmitter glutamate from the extracellular fluid studied in vivo by microdialysis and ¹³C-NMR. *J. Neurochem.* 83 (3), 682–695. doi:10.1046/j.1471-4159.2002.01161.x.
- Kauppinen, R.A., Williams, S.R., 1991. Nondestructive detection of glutamate by ¹H NMR spectroscopy in cortical brain slices from the guinea pig: evidence for changes in detectability during severe anoxic insults. *J. Neurochem.* 57 (4), 1136–1144. doi:10.1111/j.1471-4159.1991.tb08271.x.
- Kauppinen, R.A., Pirttilä, T.R.M., Auriola, S.O.K., Williams, S.R., 1994. Compartmentation of cerebral glutamate in situ as detected by ¹H/¹³C NMR. *Biochem. J.* 298, 121–127. doi:10.1042/bj2980121. (Pt1)
- Kim S, Stephenson MC, Morris PG, Jackson SR, 2014. tDCS-induced alterations in GABA concentration within primary motor cortex predict motor learning and motor memory: a 7 T magnetic resonance spectroscopy study. *Neuroimage* 99 (100), 237–243. doi:10.1016/j.neuroimage.2014.05.070.
- Kobayashi, R., Kitano, K., 2016. Impact of slow K⁺ currents on spike generation can be described by an adaptive threshold model. *J. Comp. Neurosci.* 40, 347–362. doi:10.1007/s10827-016-0601-0.
- Kupers, R., Danielsen, ER, Kehlet, H, Christensen, R, Thomsen, C., 2009. Painful tonic heat stimulation induces GABA accumulation in the prefrontal cortex in man. *Pain* 142 (1–2), 89–93. doi:10.1016/j.pain.2008.12.008.
- Levy, L.M., Ziemann, U., Chen, R., Cohen, L.G., 2002. Rapid modulation of GABA in sensorimotor cortex induced by acute deafferentation. *Ann. Neurol.* 52 (6), 755–761. doi:10.1002/ana.10372.
- Li, D., Zhu, Y., Huang, H., 2020. Spike activity regulates vesicle filling at a glutamatergic synapse. *J. Neurosci.* 40 (26), 4972–4980. doi:10.1523/JNEUROSCI.2945-19.2020.
- Liebetanz, D, Nitsche, MA, Tergau, F, Paulus, W., 2002. Pharmacological approach to the mechanisms of transcranial DC-stimulation-induced after-effects of human motor cortex excitability. *Brain* 125 (Pt 10), 2238–2247. doi:10.1093/brain/awf238.
- Lin, Y., Stephenson, M.C., Xin, L., Napolitano, A., Morris, P.G., 2012. Investigating the metabolic changes due to visual stimulation using functional proton magnetic resonance spectroscopy at 7 T. *J. Cereb. Blood Flow Metab.* 32 (8), 1484–1495. doi:10.1038/jcbfm.2012.33.
- Malerba, P., Straudi, S., Fregni, F., Bazhenov, M., Basaglia, N., 2017. Using biophysical models to understand the effect of tDCS on neurorehabilitation: searching for optimal covariates to enhance poststroke recovery. *Front. Neurol.* 8 (58), 1–13. doi:10.3389/fneur.2017.00058.
- Mangia, S, Tkáč, I, Gruetter, R, Van de Moortele, PF, Maraviglia, B, Uğurbil, K, 2006. Sustained neuronal activation raises oxidative metabolism to a new steady-state level: evidence from ¹H NMR spectroscopy in the human visual cortex. *J Cereb Blood Flow Metab* 27 (5), 1055–1063. doi:10.1038/sj.jcbfm.9600401.
- Mangia, S, Giove, F, Tkáč, I, Logothetis, N.K., Henry, P.G., Olman, C. A., Maraviglia, B., Di Salle, F., Uurbil, K., 2009. Metabolic and hemodynamic events after changes in neuronal activity: current hypotheses, theoretical predictions and in vivo NMR experimental findings. *J. Cereb. Blood Flow Metab.* 29 (3), 441–463. doi:10.1038/jcbfm.2008.134.
- Mangia, S., Giove, F., DiNuzzo, M., 2012. Metabolic pathways and activity-dependent modulation of glutamate concentration in the human brain. *Neurochem. Res.* 37 (11), 2554–2561. DOI: 0.1007/s11064-012-0848-4.
- Marreiros, A.C., Daunizeau, J., Kiebel, S.J., Friston, K.J., 2008. Population dynamics: variance and the sigmoid activation function. *Neuroimage* 42 (1), 147–157. doi:10.1016/j.neuroimage.2008.04.239.
- Marreiros, A., Kiebel, S.J., Daunizeau, J., Harrison, L.M., Friston, K.J., 2009. Population dynamics under the laplace assumption. *Neuroimage* 44 (3), 701–714. doi:10.1016/j.neuroimage.2008.10.008.
- Martínez-Maestro, M, Labadie, C, Möller, HE., 2019. Dynamic metabolic changes in human visual cortex in regions with positive and negative blood oxygenation level-dependent response. *J. Cereb. Blood Flow Metab.* 39 (11), 2295–2307. doi:10.1177/0271678X18795426.
- Martin D., Tobin A., 2000. Mechanisms controlling GABA synthesis and degradation in the brain IN GABA in the nervous system: the view at fifty years, ed. D Martin, R Olsen, pp. 25–41: LWW
- Mason, S., 2017. Lactate shuttles in neuroenergetics - homeostasis, allostasis and beyond. *Front. Neurosci.* 11, 43. doi:10.3389/fnins.2017.00043.
- Mekle, R., Kühn, S., Pfeiffer, H., Aydin, S., Schubert, F., Ittermann, B., 2017. Detection of metabolite changes in response to a varying visual stimulation paradigm using short-T₁ MRS at 7 T. *NMR Biomed.* 30 (2). doi:10.1002/nbm.3672.
- Mody, I., De Koninck, Y., Otis, T.S., Soltesz, I., 1994. Bridging the cleft at GABA synapses in the brain. *Trends Neurosci.* 17(12), 517–525. doi: 10.1016/0166-2236(94)90155-4.
- Molae-Ardekani, B., Benquet, P., Bartolomei, F., Wendling, F., 2010. Computational modeling of high-frequency oscillations at the onset of neocortical partial seizures: from 'altered structure' to 'dysfunction'. *Neuroimage* 52 (3), 1109–1122. doi:10.1016/j.neuroimage.2009.12.049.
- Molae-Ardekani, B., Márquez-Ruiz, J, Merlet, I, Leal-Campanario, R, Gruart, A, Sánchez-Campusano, R, Birot, G, Ruffini, G, Delgado-García, JM, Wendling, F, 2021. Effects of transcranial Direct Current Stimulation (tDCS) on cortical activity: a computational modeling study. *Brain Stimul* 6 (1), 25–39. doi:10.1016/j.brs.2011.12.006.
- Mountcastle, V.B., 1997. The columnar organization of the neocortex. *Brain* 120, 701–722. doi:10.1093/brain/120.4.701.
- Mullins, P. G., Rowland, L.M., Jung, R.E., Sibbitt Jr., W.L., 2005. A novel technique to study the brain's response to pain: proton magnetic resonance spectroscopy. *Neuroimage* 26 (2), 642–646. doi:10.1016/j.neuroimage.2005.02.001.
- Mullins, P.G., 2018. Towards a theory of functional magnetic resonance spectroscopy (fMRS): a meta-analysis and discussion of using mrs to measure changes in neurotransmitters in real time. *Scand. J. Psychol.* 59, 91–103. doi:10.1111/sjop.12411.
- Olsen, R.W., DeLorey, T.M., 1999. Chapter 16. GABA and Glycine in: Basic neurochemistry: Molecular, cellular and medical aspects, editors: Siegel GJ, Agranoff BW, Albers RW, et al. 6th edition. Philadelphia: Lippincott-Raven.
- Otis, T.S., Wu, Y.C., Trussell, L.O., 1996. Delayed clearance of transmitter and the role of glutamate transporters at synapses with multiple release sites. *J. Neurosci.* 16 (5), 1634–1644. doi:10.1523/JNEUROSCI.16-05-01634.1996.
- Patel, H.J., Romanzetti, S., Pellicano, A., Nitsche, M.A., Reetz, K., Binkofski, F., 2019. Proton magnetic resonance spectroscopy of the motor cortex reveals long term GABA change following anodal transcranial direct current stimulation. *Sci. Rep.* 9 (1), 2807. doi:10.1038/s41598-019-39262-7.
- Petroff, O.A.C., Burlina, A.P., Black, J., Prichard, J.W., 1992. Quantitative analysis of rat synaptosomes and cerebrum using high-resolution ¹H magnetic resonance spectroscopy. *Clin. Chim. Acta* 206 (1–2), 137–146. doi:10.1016/0009-8981(92)90014-H.
- Petroff, O.A., Errante, L.D., Rothman, D.L., Kim, J.H., Spencer, D.D., 2002. Glutamate-glutamine cycling in the epileptic human hippocampus. *Epilepsia* 43 (7), 703–710. doi:10.1046/j.1528-1157.2002.38901.x.
- Petroff, O.A.C., 2002. GABA And glutamate in the human brain. *Neuroscientist* 8 (6), 562–573. doi:10.1177/1073858402238515.
- Pirttilä, TR, Hakumäki, JM, Kauppinen, RA., 1993. ¹H nuclear magnetic resonance spectroscopy study of cerebral glutamate in an ex vivo brain preparation of guinea pig. *J. Neurochem.* 60 (4), 1274–1282. doi:10.1111/j.1471-4159.1993.tb03287.x.
- Pospischil, P., Toledo-Rodriguez, M., Monier, C., Piwkowska, Z., Bal, T., Frégnac, Y., Markram, H., Destexhe, A., 2008. Minimal Hodgkin-Huxley type models for different classes of cortical and thalamic neurons. *Biol. Cybern.* 99, 427–441. doi:10.1007/s00422-008-0263-8.
- Rae, C.D., 2014. A guide to the metabolic pathways and function of metabolites observed in human brain ¹H magnetic resonance spectra. *Neurochem. Res.* 39 (1), 1–36. doi:10.1007/s11064-013-1199-5.
- Rahman, A., Lafon, B., Bikson, M., 2015. Multilevel computational models for predicting the cellular effects of noninvasive brain stimulation. *Prog. Brain Res.* 222, 25–40. doi:10.1016/bs.pbr.2015.09.003.
- Ramadan, S., Lin, A., Stanwell, P., 2013. Glutamate and glutamine: a review of in vivo MRS in the human brain. *NMR Biomed.* 26(12), 1630–1646. doi:10.1002/nbm.3045.
- Rodriguez, R., Tuckwell, H.C., 1996. Statistical properties of stochastic nonlinear dynamical models of single spiking neurons and neural networks. *Phys. Rev. E* 54, 5585. doi:10.1103/PhysRevE.54.5585.
- Rodriguez, R., Tuckwell, H. C., 1998. Noisy spiking neurons and networks: useful approximations for firing probabilities and global behavior. *BioSystems* 48 (1–3), 187–194. doi:10.1016/S0303-2647(98)00065-3.
- Rothman, D.L., Sibson, N. R., Hyder, F., Shen, J., Behar, K.L., Shulman, R. G., 1999. In vivo nuclear magnetic resonance spectroscopy studies of the relationship between the glutamate-glutamine neurotransmitter cycle and functional neuroenergetics. *Philos. Trans. R. Soc. Lond. B Biol. Sci.* 354, 1165–1177. doi:10.1098/rstb.1999.0472.
- Rothman, D. L., Behar, K.L., Hyder, F., Shulman, R. G., 2003. In vivo NMR studies of the glutamate neurotransmitter flux and neuroenergetics: implications for brain function. *Ann. Rev. Physiol.* 65 (1), 401–427. doi:10.1146/annurev.physiol.65.092101.142131.
- Sánchez-León, C. A., Cordones, I., Ammann, C., Ausín, J. M., Gómez-Climent, M. A., Carretero-Guillén, A., Sánchez-Garrido Campos, G., Gruart, A., Delgado-García, J. M., Cheron, G., Medina, J. F., Márquez-Ruiz, J., 2021. Immediate and after effects of transcranial direct-current stimulation in the mouse primary somatosensory cortex. *Sci. Rep.* 11 (3123). doi:10.1038/s41598-021-82364-4.
- Südhof, T.C., 1999. Composition of Synaptic Vesicles. In: Siegel GJ, Agranoff BW, Albers RW, et al., editors. *Basic Neurochemistry: Molecular, Cellular and Medical Aspects*. 6th edition. Philadelphia: Lippincott-Raven; 1999.
- Schaller, B., Mekle, R., Xin, L., Kunz, N., Gruetter, R., 2013. Net increase of lactate and glutamate concentration in activated human visual cortex detected with

- magnetic resonance spectroscopy at 7 Tesla. *J. Neurosci. Res.* 91 (8), 1076–1083. doi:10.1002/jnr.23194.
- Schousboe, A., 1981. Transport and metabolism of glutamate and gaba in neurons and glial cells. *Intl. Rev. Neurobiol.* 22, 1–45. doi:10.1016/s0074-7742(08)60289-5.
- Shen, J., Petersen, K.F., Behar, K.L., Brown, P., Nixon, T.W., Mason, G.F., Petroff, O., Shulman, G.I., Shulman, R.G., Rothman, D.L., 1999. Determination of the rate of the glutamate/glutamine cycle in the human brain by in vivo ¹³C NMR. *Proc. Natl. Acad. Sci. U.S.A.* 96 (14), 8235–8240. doi:10.1073/pnas.96.14.8235.
- Sibson, N.R., Dhankhar, A., Mason, G. F., Behar, K.L., Rothman, D.L., Shulman, R.G., 1997. In vivo ¹³C NMR measurements of cerebral glutamine synthesis as evidence for glutamate glutamine cycling. *Proc. Natl. Acad. Sci. U.S.A.* 94 (6), 2699–2704. doi:10.1073/pnas.94.6.2699.
- Sibson, N.R., Dhankhar, A., Mason, G. F., Rothman, D.L., Behar, K.L., Shulman, R.G., 1998. Stoichiometric coupling of brain glucose metabolism and glutamatergic neuronal activity. *Proc. Natl. Acad. Sci. U.S.A.* 95, 316–321. doi:10.1073/pnas.95.1.31.
- Somogyi, P., Tamas, G., Lujan, R., Buhl, E.H., 1998. Salient features of synaptic organisation in the cerebral cortex. *Brain Res. Revs.* 26 (2–3), 113–115. doi:10.1016/s0165-0173(97)00061-1.
- Song, Y., Yao, M., Kemprecos, H., Byrne, A., Xiao, Z., Zhang, Q., Singh, A., Wang, J., Chen, Z., 2021. Predictive coding models for pain perception. *J. Comp. Neurosci.* 49, 107–127. doi:10.1007/s10827-021-00780-x.
- Sonnenwald, U., McKenna, M., 2002. Metabolic compartmentation in cortical synaptosomes: influence of glucose and preferential incorporation of endogenous glutamate into GABA. *Neurochem. Res.* 27 (1), 43–50. doi:10.1023/A:1014846404492.
- Sonnenwald, U., Westergaard, N., Schousboe, A., Svendsen, JS, Unsgård, G, Petersen, SB, 1993. Direct demonstration by [¹³C]NMR spectroscopy that glutamine from astrocytes is a precursor for GABA synthesis in neurons. *Neurochem. Int.* 22 (1), 19–29. doi:10.1016/0197-0186(93)90064-c.
- Sonnenwald, U., 2014. Glutamate synthesis has to be matched by its degradation where do all the carbons go? *J. Neurochem.* 131 (4), 399–406. doi:10.1111/jnc.12812.
- Stagg, C. J., Best, J.G., Stephenson, M. C., O’Shea, J., Wylezinska, M., Kincses, T., Morris, P. G., Matthews, P. M., Johansen-Berg, H., 2009. Polarity-sensitive modulation of cortical neurotransmitters by transcranial stimulation. *J. Neurosci.* 29 (16), 5202–5206. doi:10.1523/JNEUROSCI.4432-08.2009.
- Stagg, C. J., Bachtiar, V., Johansen-Berg, H., 2011. The role of GABA in human motor learning. *Curr. Biol.* 21 (6), 480–484. doi:10.1016/j.cub.2011.01.069.
- Stevens, C. F., Tsujimoto, T., 1995. Estimates for the pool size of releasable quanta at a single central synapse and for the time required to refill the pool. *Proc. Natl. Acad. Sci. U.S.A.* 92 (3), 846–849. doi:10.1073/pnas.92.3.846.
- Szentágothai, J., 1983. The modular architectonic principle of neural centers. *Rev. Phys. Biochem. Pharmacol.* 98, 11–61. doi:10.1007/BFb0033866.
- Taylor, R., Neufeld, R., Schaefer, B., Densmore, M., Rajakumar, N., Osuch, E., Williamson, P., Théberge, J., 2015. Functional magnetic resonance spectroscopy of glutamate in schizophrenia and major depressive disorder: anterior cingulate activity during a color-word stroop task. *NPJ Schizophr* 1, 15028. doi:10.1038/npjpsz.2015.28.
- Théberge, J., Bartha, R., Drost, D., Menon, R., Malla, A., Takhar, J., Neufeld, R., Rogers, J., Pavlosky, W., Schaefer, B., Densmore, M., Al-Semaan, Y., Williamson, P., 2002. Glutamate and glutamine measured with 4.0 T proton MRS in never-treated patients with schizophrenia and healthy volunteers. *Am. J. Psychiatry* 159 (11), 1944–1946. doi:10.1176/appi.ajp.159.11.1944.
- Thompson, S. M., 1994. Modulation of inhibitory synaptic transmission in the hippocampus. *Progr. Neurobiol.* 42 (5), 575–609. doi:10.1016/0301-0082(94)90044-2.
- Tranchina, D., Nicholson, C., 1986. A model for the polarization of neurons by extrinsically applied electric fields. *Biophys. J.* 50 (6), 1139–1156. doi:10.1016/S0006-3495(86)83558-5.
- Tsodyks, M., Markram, H., 1997. The neural code between neocortical pyramidal neurons depends on neurotransmitter release probability. *Proc. Natl. Acad. Sci. U.S.A.* 94 (2), 719–723. doi:10.1073/pnas.94.2.719.
- Tsodyks, M., Pawelzik, K., Markram, H., 1998. Neural networks with dynamic synapses. *Neural. Comput.* 10 (4), 821–835. doi:10.1162/089976698300017502.
- Wilson, H.R., Cowan, J.D., 1972. Excitatory and inhibitory interactions in localized populations of model neurons. *Biophys. J.* 12 (1), 1–24. doi:10.1016/S0006-3495(72)86068-5.
- Wilson, H.R., Cowan, J.D., 1973. A mathematical theory of the functional dynamics of cortical and thalamic nervous tissue. *Kybernetik* 13, 55–80. doi:10.1007/BF00288786.
- Wilson, H.R., 2003. Computational evidence for a rivalry hierarchy in vision. *Proc. Natl. Acad. Sci. U.S.A.* 100 (24), 14499–14503. doi:10.1073/pnas.2333622100.
- Zandt, B.J., Visser, S., van Putten, M., ten Haken, B., 2014. A neural mass model based on single cell dynamics to model pathophysiology. *J. Comp. Neurosci.* 37, 549–568. DOI: 10.1007/s10827-014-0517-5.
- Zhao, X., Ding, J., Pan, H., Zhang, S., Pan, D., Yu, H., Ye, Z., Hua, T., 2020. Anodal and cathodal tDCS modulate neural activity and selectively affect GABA and glutamate syntheses in the visual cortex of cats. *J. Physiol.* 598, 3727–3745. doi:10.1113/JP279340.
- Zou, Q., Destexhe, A., 2007. Kinetic models of spike-timing dependent plasticity and their functional consequences in detecting correlations. *Biol Cybern* 97 (1), 81–97. doi:10.1007/s00422-007-0155-3.